Spatially Resolved Proteomic Profiling Uncovers Structural and Functional Regulators of the Axon Initial Segment

Wei Zhang[1,2], Yu Fu[1], Luxin Peng[1], Yuki Ogawa[3], Xinyue Zhou[2], Matthew N. Rasband[3], Peng Zou[1,2,4*]

1. College of Chemistry and Molecular Engineering, Synthetic and Functional Biomolecules Center, Beijing National Laboratory for Molecular Sciences, PKU-IDG/McGovern Institute for Brain Research, Key Laboratory of Bioorganic Chemistry and Molecular Engineering of Ministry of Education, Peking University, Beijing, 100871, China
2. Academy for Advanced Interdisciplinary Studies, PKU-Tsinghua Center for Life Science, Peking University, Beijing 100871, China
3. Department of Neuroscience, Baylor College of Medicine, Houston, TX, USA
4. Chinese Institute for Brain Research (CIBR), Beijing 102206, China

[*] Correspondence: zoupeng@pku.edu.cn (P.Z.)

ABSTRACT

Axon initial segments (AISs) are specialized neuronal compartments crucial for action potential generation and neuronal polarity. However, a detailed understanding of the mechanisms regulating AIS structure and function has been hindered by an incomplete knowledge of its molecular composition. Here, we profile the AIS proteome and its dynamic changes in-depth during neuronal maturation. Our method capitalizes on antibody targeted proximity labeling with subcellular spatial specificity in fixed primary neurons. Among the AIS proteins labeled, we identified novel AIS components, including PHGDH and SCRIB. PHGDH and SCRIB are highly enriched in the AIS both *in vitro* and *in vivo,* and exhibit a periodic architecture like the axonal spectrin-based cytoskeleton. Furthermore, we show that neuronal PHGDH activity is necessary for AIS integrity and action potential initiation. This powerful and flexible approach defines the AIS proteome and provides a rich resource to elucidate the mechanisms regulating AIS structure and

function.

KEYWORDS

axon initial segment, proteomics, proximity labeling, PHGDH, SCRIB, neuron

INTRODUCTION

The axon initial segment (AIS) is the 20~60 μm long proximal region of the axon responsible for action potential generation and maintenance of neuronal polarity [1,2]. Changes in the molecular composition of the AIS, its length, or position can alter neuronal excitability [3-5]. Disruption of the AIS causes axons to acquire dendritic characteristics [6,7]. Recent studies show that AIS disruption occurs in many neurological diseases, such as autism, Alzheimer's disease, stroke, bipolar disorder and schizophrenia [8]. Rescuing AIS integrity and function can ameliorate neurological symptoms in Alzheimer's disease and Angelman Syndrome mouse models [9,10]. However, our incomplete knowledge of AIS components hinders our understanding of the structural and functional regulation of AIS in health and disease.

Axon initial segments consist of a specialized extracellular matrix, clustered cell adhesion molecules (CAMs) and voltage gated ion channels, and a unique cytoskeleton. Among the known AIS proteins, the scaffolding protein ankyrinG (AnkG) is the master organizer for AIS assembly and maintenance [8]. AnkG links membrane proteins to the actin cytoskeleton through a tetramer consisting of βIV and αII-spectrin, and to the microtubule cytoskeleton through the end binding proteins EB1 and EB3 [11]. At the AIS, microtubules form parallel fascicles thought to be organized by TRIM46 [12,13]. As the site for axonal action potential initiation, AIS also have voltage gated sodium (e.g. Nav1.2), potassium (e.g. Kv7) and calcium channels (e.g. Cav2), arranged to regulate spike generation, pattern and shape [14]. NF186, a neuron-specific isoform of the CAM neurofascin (NFASC), assembles and links extracellular matrix molecules (e.g. Brevican) to the AIS cytoskeleton [15]. In

addition, some synaptic proteins (e.g. Gephyrin), cisternal organelle molecules (e.g. Synaptopodin) and a Kv1 channel complex (e.g. PSD93) can also be found at the AIS [16].

The combination of enzyme-mediated proximity-dependent biotinylation and mass spectrometry-based quantitative proteomics has emerged as a powerful tool to elucidate endogenous protein complexes in subcellular domains. Two main categories of proximity labeling methods have been developed based on enzymes used for catalysis: biotin ligase-based proximity labeling (e.g. BioID and TurboID) and peroxidase-based proximity labeling (e.g. HRP and APEX2). Pioneering experiments using AIS-targeted BioID were recently used to uncover a partial AIS proteome. However, the experiments were restricted to cytoplasmic AIS proteins and the labeling radius of BioID is confined to 10 nm [17].

Here, we report the development of **a**ntibody targeted **p**roximity **l**abeling in fixed neurons, together with a multiple ratiometric analysis strategy to define the **AIS** proteome (APL-AIS). The APL-AIS method takes advantage of the sub-micrometer labelling radius of peroxidase-mediated protein biotinylation in permeabilized and fixed samples [18]. Antibody targeted proximity labeling has been previously used to map mitochondrial matrix, lamin A/C interactome, nuclear speckles, and proximal proteins of histone modifications in cell lines [19-21]. It targets endogenous baits without requiring genetic manipulation, thus avoiding artifacts from over-expression or fusion proteins with altered subcellular localization.

We applied quantitative ratiometric proteomics with multiple controls to elucidate AIS proteins [22,23]. APL-AIS profiling at DIV7, 14 and 21 (days *in vitro*) portrayed the dynamic changes of AIS components along neuronal development. Subsequent validation confirmed the identification of novel AIS enriched proteins, including phosphoglycerate dehydrogenase (PHGDH) and the tumor-suppressor protein scribble (SCRIB). Functional studies of PHGDH revealed its involvement in AIS integrity and neuronal excitability. Together, our experiments define known and some new AIS components, which may open

new opportunities to understand the molecular mechanisms regulating AIS structure and function.

RESULTS

Development of antibody targeted proximity labeling at the AIS

The CAM NF186 is highly and stably localized in the AIS [24,25], therefore we used NF186 for antibody targeted proximity labeling at the AIS. As illustrated in Figure 1A, cultured cortical neurons were fixed and labeled using antibodies to restrict horseradish peroxidase (HRP) to the AIS. HRP-mediated proximity-dependent biotinylation is triggered with the addition of biotin-phenol substrates and hydrogen peroxide. Biotinylation is evaluated with fluorescent streptavidin and immunoblot analysis. Following enrichment via affinity purification, biotinylated proteins are digested with trypsin and identified via quantitative LC-MS/MS analysis.

We optimized antibody dilutions, H_2O_2 concentration, reaction time and different biotin-phenol (BP) probes in the proximity labeling system using mature fixed cortical neurons (Figure S1). The proper dilution of antibodies increased the proximity labeling specificity, and 100 μM H_2O_2 significantly improved the labeling selection and efficiency in 1 min. Previous studies showed the peroxidase substrate BP2 performs well for labeling of cytosolic protein complexes (Figure S1E) [26], while the substrates BA1 and BA2 exhibit higher reactivity towards nucleic acids (Figure S1E) [27]. Our analysis revealed biotin-phenol (BP) as the most efficient and specific substrate for *in vitro* AIS proximity labeling. We employed these optimized parameters and found strongly biotinylated proteins localized in the AIS (Figure 1B). Through imaging, we also tested other AIS-directed antibodies for proximity labeling, including antibodies against AnkG and TRIM46. In our hands, NFASC targeted proximity labeling exhibited the best performance, with less background and highly specific biotinylation of AIS (data not shown).

To remove background signal arising from non-specific binding of antibodies, experiments omitting the primary antibody (i.e. anti-NFASC) were used as the negative control. To quantify the level of protein enrichment at the AIS, we chose NeuN and MAP2 to define soma and somatodendritic domains, respectively. NeuN localizes in the nuclei and cytoplasm of neurons [28,29], while MAP2 is a microtubule-associated protein that is widely distributed throughout the soma and dendrites [5,30]. Fluorescence microscopy showed highly colocalized biotinylation and immunofluorescence labeling for both NeuN and MAP2 (Figure 1B). Thus, we applied the same experimental workflow to anti-NeuN and anti-MAP2 defined compartments; these served as the references for ratiometric analysis of the AIS proteome.

Biochemical characterization by streptavidin-HRP blot and silver staining showed successful protein biotinylation from anti-NFASC, anti-NeuN, and anti-MAP2 proximity labeling experiments (Figure 1C). As expected, the negative control sample omitting primary antibody yielded significantly less signal; any background signal presumably arose from detection of endogenously biotinylated proteins. Notably, the biotinylation signal was stronger in anti-NeuN and anti-MAP2 reference samples compared to the anti-NFASC sample, which may reflect the higher abundance of and larger volume occupied by NeuN and MAP2.

To quantitatively compare protein abundance between samples, we designed dimethyl proteomics using the following sets of ratiometric MS experiments: 1) anti-NFASC vs. no primary antibody; 2) anti-NFASC vs. anti-NeuN; and 3) anti-NFASC vs. anti-MAP2. The first experiment served to remove background labeling arising from non-specific staining of secondary antibody-HRP conjugates, endogenous biotinylated proteins, and non-specific protein adsorption on streptavidin-coated beads. The next two experiments allowed distinction of AIS-specific proteins from those broadly distributed across the cell. For each set of experiments, three biological replicates were performed on cultured cortical neurons at DIV14 (Figure 1D).

A total of 568 proteins were identified after a stringent cut-off analysis (see Methods), among which several known AIS proteins, including TRIM46, AnkG, and NFASC were highly enriched in our dataset (Figure 1E; Table S1). Interestingly, serine biosynthesis enzyme PHGDH, also appeared highly enriched, almost at the same level as NFASC. On the other hand, we also noticed the low enrichment of EB1 and SEPTIN5, which were previously reported as AIS proteins. Indeed, these two proteins are widely expressed in neurons and no relatively higher signal was observed in the AIS [11,17], which may explain their lack of specific enrichment in our experiments. Taken together, these results demonstrate that the AIS proteome can be defined using our APL-AIS methods.

Identification of AIS proteome at DIV14

Building upon the success of our pilot APL-AIS experiments, we next sought to improve the quality of our proteomic dataset through implementing the following changes in the workflow (Figure 2A and 2B): 1) to improve protein abundance quantitation across multiple samples, we introduced Tandem Mass Tag (TMT) 10-plex isobaric tags to label tryptic peptides [31], 2) to achieve higher coverage in labeled peptides, we reduced sample complexity by fractionating peptides prior to loading onto the LC-MS/MS, and 3) to further improve spatial specificity, we added anti-SMI312 targeted axon proximity labeling to the reference samples (in addition to NeuN and MAP2) (Figure 2A). Confocal fluorescence imaging analysis confirmed axonal localization of anti-SMI312 targeted protein biotinylation (Figure S2).

Streptavidin-HRP blot analysis confirmed successful enrichment of biotinylated proteins across antibody targeted proximity labeling samples, whereas negative control samples yielded negligible signal (Figure S3). A total of 2,755 proteins with at least 2 unique peptides were detected in the 10-plex TMT MS experiment (Figure 2C). The MS intensity was highly reproducible between replicates (Figure 2D). We then used the following data analysis pipeline to refine our AIS proteome (Figure 2C). We first identified

biotinylated proteins by comparing the MS intensities of anti-NFASC samples against negative controls (-BP and -1Ab). By applying a cutoff ratio of 2, we obtained a list of 1403 biotinylated proteins. For each protein in this raw list, we calculated the ratios of its MS intensities between anti-NFASC samples versus those in the reference samples (+NeuN, +MAP2, and +SMI312). We then ranked proteins according to their averaged MS intensity ratios (+NF/+NeuN, +NF/+MAP2, and +NF/+SMI312) (Figure 2E) and calculated their averaged rank scores (Figure 2F). Notably, our results included many known AIS proteins (Figure 2E, 2F and 4A), including extracellular proteins (e.g. Brevican and Versican), CAMs (e.g. NFASC and NRCAM), cytoplasmic proteins (e.g. NDEL1 and LIS1), and cytoskeletal or cytoskeleton-associated proteins (e.g. βIV-spectrin, αII-spectrin and TRIM46). This broad coverage of both cytoplasmic and cell surface proteins indicates the labeling radius of optimized APL-AIS is suitable to capture proteins across the entire AIS. Importantly, our dataset included many voltage-gated ion channels, such as sodium channels (e.g. Nav1.2 and Navβ2), potassium channels (e.g. Kv7.2, Kv1.2, Kv2.1 and Kvβ2), and calcium channels (e.g. Cav2.1 and Cav2.2), consistent with their roles in regulating action potential initiation and shape [14].

AIS candidates (1403) compared against each reference control exhibited their relative expression in the AIS versus soma, somatodendritic, or axonal domains (Figure 2E; Table S2). AIS highly expressed proteins (NFASC, Nav1.2, AnkG, TRIM46 and βIV-spectrin) were always ranked at the top, while more widely expressed AIS proteins differentiated according to their relative expression level in subcellular domains, such as the microtubule protein TUBA4A or microtubule related protein MAP6 (Figure 2E) [17]. To better define AIS enriched proteins, we applied averaged rank scores to re-list the known and putative AIS proteins (Figure 2F; Table S2). Consistently, known AIS highly expressed proteins were found among the top 5. More widely expressed proteins, such as F-actin monooxygenase MICAL3 (ranked 371) and Rho GTPase activating protein ARHGAP21 (ranked 455), were not as highly ranked [17].

To obtain a high-confidence AIS proteome list, we took the overlap of the top 200 proteins in each list of MS intensity ratios (+NF/+NeuN, +NF/+MAP2, and +NF/+SMI312). The resulting high-confidence list contained 71 proteins (Figure 2C and 2G; Table S2). Gene Ontology cellular compartment analysis revealed an over-representation of AIS and node of Ranvier terms due to the similar compositions of these two compartments (Figure 2H). The remaining top 10 GOCC terms were consistent with AIS characteristics and its endocytosis functions [16,32]. The specificity was further confirmed by Gene Ontology molecular function analysis with over-representation of sodium ion binding, microtubule binding and spectrin binding terms (data not shown).

Mapping AIS proteome across neuronal maturation

The AIS is developmentally and physiologically dynamic [25,33]. To determine dynamic developmental changes in the AIS proteome, we performed APL-AIS at DIV7, DIV14, and DIV21. Two parallel 10-plex TMT experiments were performed and DIV14 samples were used as a reference to bridge DIV7 and DIV21 samples (Figure 3A).

We first analyzed the DIV7 AIS proteome. Parallel analysis of 1532 common proteins revealed highly reproducible protein quantifications (R^2= 0.94) (Figure 3B). After stringent filtering (Figure S4A), we obtained 1407 biotinylated proteins. Rank analysis revealed the specificity of our DIV7 AIS dataset with top ranked AIS proteins including AnkG, TRIM46, βIV-spectrin, NFASC and Nav1.2 (Figure 3C). Other AIS proteins were more widely dispersed, possibly due to different expression levels and labeling efficiencies. Through integrating average rank scores of AIS versus soma or somatodendrites, we obtained a final ranked putative AIS proteome including AIS proteins in top positions (Figure 3D; Table S3). Using the same workflow (Figure S4B), we identified 1738 biotinylated proteins at DIV21. Parallel analysis of anti-NFASC replicates showed highly reproducible protein quantifications (R^2= 0.98) (Figure 3E), and rank scores of AIS versus soma or somatodendritic proteins (Figure 3F) resulted in AIS proteins being consistently at the top

(Figure 3G; Table S3). Some AIS proteins, such as Synaptopodin (SYNPO) and PSD-93 (PSD93) were ranked lower (Figure 3G) [34,35].

Comparing biotinylated proteins between DIV7 and DIV14 in 10-plex TMT revealed 173 proteins only present at DIV7 and 152 proteins only present at DIV14, among which there were only two previously reported AIS proteins: Gephyrin and microtubule protein TUBA4A (Figure S4D). DIV14 samples in the two parallel 10-plex TMT experiments presented a very high reproducibility among biological replicates (Figure S4E) and enrichment of known AIS proteins (Figure S4F), allowing us to compare protein relative expression in three stages together. To identify the core set of putative AIS proteins during development, DIV7, 14, 21 and the prior DIV14 datasets (Figure 2) were combined, which generated a total of 549 common proteins (Figure 3H). Among these, 534 proteins showed 20% changes in any one pair comparison of three time points were used for heatmap clustering. Six clusters were generated with distinct expression patterns (Figure 3I; Table S3). 51.7% proteins were gradually upregulated and 4.1% proteins were gradually downregulated along neuronal development (Figure 3J). The highest expression level at DIV21 included 83.5% of proteins, while at DIV7 it only 15.3% of proteins were present.

Consistently, the previously reported AIS proteins exhibited the highest expression level at DIV21, including NFASC (*Nfasc*), AnkG (*Ank3*), Nav1.2 (*Scn2a*), and βIV-spectrin (*Sptbn4*), while TRIM46 (*Trim46*) decreased along neuronal development (Figure 3K). Quantitative analysis revealed the fold changes and statistical significance between stages (Table S3). For example, microtubule-associated proteins MAP1A (*Map1a*), MAP6 (*Map6*), sodium/potassium-transporting ATPase subunit alpha-1 (*Atp1a1*) and casein kinase II subunit alpha (*Csnk2a1*) exhibited a more than two-fold significant change from DIV7 to 14 (Figure 3L). From DIV14 to 21, more microtubule or microtubule-associated proteins like TUBB5 (*Tubb5*), TUBB3 (*Tubb3*) and EB3 (*Mapre3*) significantly increased, while calcium/calmodulin-dependent protein kinase KCC2D (*Camk2d*) and KCC2A (*Camk2a*) also had more than two-fold changes (Figure 3M). Comparison between DIV7

and 21 revealed more components with a two-fold significant increase, including the AIS proteins NFASC (*Nfasc*), Nav1.2 (*Scn2a*) and GABA(A) receptor subunit gamma-2 (*Gabrg2*), while TRIM46 (*Trim46*) showed a two-fold significant decrease (Figure 3N), further demonstrating the dynamic nature of AIS composition along neuronal development.

PHGDH and SCRIB are bona fide AIS enriched proteins

To identify novel AIS polarized proteins, we examined top ranked proteins identified at DIV14 to assess their subcellular localization in neurons (Figure 4A). Among these, PHGDH was a top ranked candidate in both the 10-plex TMT proteomics and preliminary dimethyl proteomics (Figure 4A and 1E). Pathogenic variants in *Phgdh* are associated with severe neurological disorders including congenital microcephaly and psychomotor retardation. PHGDH is preferentially expressed in glial cells and is reported to mediate the biosynthesis of L-serine to indirectly promote neuronal survival and differentiation [36]. However, our results also revealed prominent PHGDH immunostaining in the AIS with much weaker labeling of dendrites in DIV12-15 cortical neurons (Figure 4B). This polarized distribution occurred at DIV6 after AIS formation (Figure 4C and 4D; Figure S5A), suggesting PHGDH is recruited to the AIS by other AIS proteins like AnkG. In addition, a strong PHGDH signal was observed in the AIS of brain cortical slices (Figure S5C). Previous studies showed that AIS proteins are resistant to detergent extraction [37,38]. TritonX-100 treatment revealed a detergent-resistant pool of PHGDH that colocalized with AnkG at the AIS (Figure 4E). To confirm the localization of PHGDH in neurons, we used CRISPR-mediated endogenous gene tagging to knock in a smFP-V5 tag to the C-terminus of endogenous PHGDH proteins. Consistent with our immunostaining results (Figure 4B), smFP-V5-tagged PHGDH was highly enriched in the AIS of hippocampal neurons (Figure 4F).

Some AIS proteins, including voltage gated sodium channels, βIV-spectrin, NFASC and AnkG have a periodic spacing in the AIS with a distance of approximately 180~190

nm [39,40]. To test whether PHGDH exhibited a similar pattern, we used stimulated emission depletion (STED) nanoscopy to image the endogenous smFP-V5-tagged PHGDH distribution in cultured rat hippocampal neurons. A periodicity of 177.3 ± 10.7 nm was observed in the AIS of DIV21 neurons (Figure 4G), suggesting a strong association of PHGDH with previously described components of the AIS periodic cytoskeleton [39]. In summary, our data demonstrate that PHGDH is highly enriched in the AIS both *in vitro* and *in vivo*.

SCRIB (*Scrib*) is another top ranked candidate AIS protein (ranked 8 out of 1403) in our 10-plex TMT proteomic dataset. Although SCRIB has been reported as an important regulator of cortical development, spine morphology and synapse plasticity [41-43], SCRIB has not been reported at the AIS. We first sought to assess the subcellular localization of SCRIB using commercial antibodies. Consistent with previous studies, we found that SCRIB localized in dendritic spines and synapses in DIV15 cortical neurons (Figure 4H). Intriguingly, a strong signal of SCRIB could also be detected in the AIS (Figure 4H). Quantitative analysis revealed a ~4-fold (DIV6, 4.14 ± 0.31; DIV15, 4.45 ± 0.35; DIV21, 5.62 ± 0.51) higher intensity of SCRIB in the AIS than in the axon and ~3-fold (DIV6, 2.61 ± 0.12; DIV15, 2.75 ± 0.14; DIV21, 3.05 ± 0.13) higher than in the dendrites (Figure 4I and 4J). Like PHGDH, SCRIB became polarized at the AIS at DIV6, after the AIS was formed (Figure 4I and 4J; Figure S5B); SCRIB was not detectable in the proximal axon at DIV2 (Figure S5B). TritonX-100 treatment of live DIV12 neurons revealed a detergent-resistant pool of SCRIB at the AIS (Figure 4K). SCRIB was also highly enriched in the AIS in cortex (Figure S5D). SCRIB's enrichment at the AIS was further confirmed by insertion of an smFP-V5 tag into endogenous SCRIB (Figure 4F). STED imaging of smFP-V5 tagged SCRIB showed the endogenous protein exists in a periodic pattern of 189.4 ± 6.6 nm intervals in DIV16 hippocampal neurons (Figure 4G). Thus, APL-AIS reveals that SCRIB is a novel AIS enriched protein.

PHGDH regulates AIS structure and function

We focused the remainder of our studies on PHGDH since it has not been well studied in neurons. Our experiments illustrate the utility of our APL-AIS to identify proteins that regulate AIS structure and function. To determine the effects of PHGDH activity on mature AIS, we used the selective inhibitor NCT503 to block PHGDH activity and a non-active analogue PHGDH-inactive as a negative control (Inac) [44,45]. Treatment with 50 μM NCT503 for 48 h led to a 40% reduction in AIS AnkG immunoreactivity in DIV15 cortical neurons (Figure 5A and 5B). The reduction in AnkG immunoreactivity was also dose dependent (Figure S6A). Compared to controls, the treated neurons maintained their morphology based on MAP2 staining, suggesting the treatment did not affect neuronal health (Figure 5A). To test if other AIS components were also affected, we analyzed other two AIS enriched components NFASC and TRIM46 and found ~33% decrease for NFASC and ~38% decrease for TRIM46 (Figure 5C and 5D; Figure S6E). As an alternative PHGDH inhibitor, we found that 50 μM CBR5884 [45,46] also reduced AnkG, NFASC and TRIM46 immunoreactivity in the AIS without affecting neuronal morphology (Figure 5E; Figure S6E). Quantitative analysis after 48 h treatment using CBR5884 revealed a reduction of AnkG (~36%), NFASC (~36%) and TRIM46 (~43%) comparable to that caused by treatment with NCT503 (Figure 5F-H).

In addition to a reduction in AIS immunoreactivity, we also found AIS length shortening (Figure 5A and 5E; Figure S6E). Taking AnkG or NFASC signal as references, we quantified AIS length after blocking PHGDH activity for 48 h. Quantitative analysis revealed a ~28% and ~14% reduction in AIS length for AnkG and NFASC after NCT503 treatment, while neurons treated with CBR5884 had their AIS length reduced by ~10% for AnkG and ~23% for NFASC (Figure 5I-L). Remarkably, AIS integrity was disrupted after only 3 h inhibition of PHGDH activity (Figure S6F-I).

To exclude the possibility that PHGDH inhibition indirectly affects neurons through glia (i.e. astrocytes), we treated neurons with NCT503 or CBR5884 in the presence or

absence of astrocytes and found a comparable reduction in AnkG immunoreactivity and AIS length in both conditions (Figure 5M-P), suggesting that inhibition of neuronal PHGDH, rather than astrocyte PHGDH, influences AIS properties. Moreover, the consequences of PHGDH inhibition were reversible after NCT503 washout and maintenance in conditioned neuronal medium for 24 h (integrated AnkG immunofluorescence in NCT503: 65.5 ± 3.8 after 0 h vs 92.9 ± 3.7 after 24 h; AIS length in NCT503: 84.7 ± 2.2 after 0 h vs 95.6 ± 2.5 after 24 h, Figure S6J-M).

Since inhibition of PHGDH decreased the amount of AIS components and shortened AIS length, we considered that neuronal excitability could also be affected. To test this hypothesis, DIV14/15 cortical neurons were recorded after 48 h treatment with 50 μM NCT503 or its non-active analogue Inac. Consistent with altered AIS structure (Figure 6A), we found a remarkable reduction in the intrinsic excitability after treatment with NCT503 (Figure 6B). The resting potential was significantly decreased after blocking PHGDH activity (Inac: -62.65 ± 1.01 mV; NCT503: -68.06 ± 1.63 mV, unpaired t-test, p= 0.0051; Figure 6C). The decrease in intrinsic excitability was also reflected by a significant reduction of maximal rising speed (from 123.4 ± 4.36 mV/ms to 101.6 ± 5.46 mV/ms, unpaired t-test, p= 0.003; Figure 6D) and a pronounced increase of rheobase density (from 2.20 ± 0.21 pA/pF to 3.66 ± 0.423 pA/pF, Mann-Whitney, p= 0.0012; Figure 6E). Action potential measurement revealed -37.39 ± 1.37 mV voltage threshold in NCT503 treated neurons versus -39.81 ± 0.68 mV in control neurons (p= 0.0973, unpaired t-test; Figure 6F). Slight reductions in spike amplitude (Inac: 113.3 ± 1.84 mV; NCT503: 107.8 ± 2.56 mV, unpaired t-test, p= 0.08; Figure 6G) and numbers were observed (Figure 6H), albeit there was no statistical significance.

Voltage-clamp recordings further revealed a decrease of voltage-gated sodium channel current density after blocking PHGDH activity (Figure 6I). Statistical analysis showed a significant reduction of maximal voltage gated sodium channel current density (from -63.31 ± 5.75 pA/pF to -46.27 ± 4.40 pA/pF, Mann-Whitney, p = 0.0077; Figure 6J).

Consistently, the voltage threshold of voltage gated sodium channel activation was increased (from -58.86 ± 1.09 mV to -52.81 ± 1.02 mV, Mann-Whitney, p= 0.0013; Figure 6K). These data support the conclusion that inhibition of PHGDH reduces the intrinsic excitability of neurons by altering AIS properties.

DISCUSSION

Neuronal circuits rely on action potential generation and neuronal communication. The AIS plays key roles in regulating action potential initiation and maintaining neuronal polarity. Functional and structural changes of AIS in normal and pathological conditions are often associated with changes in its molecular composition. Here, we used APL-AIS to identify the AIS proteome. Our dataset included almost all known AIS components including extracellular matrix proteins, membrane proteins, and cytoskeleton-associated proteins. Notably, most voltage-gated ion channels and their accessory subunits were also identified, including Nav1.2, Navβ2, Kv2.1, Kv7.2, Kv1.2, Kvβ2, and Cav2.1 and Cav2.2 (Figure 2F). This in-depth coverage extends the findings of a previous proximity labeling study using BioID, which was designed to identify AIS cytoplasmic and cytoskeleton-associated proteins, and missed AIS cell surface proteins including Tenascin-R and many voltage-gated ion channels identified using APL-AIS [17].

Although our APL-AIS has used stringent threshold for cutoff analysis against negative controls, there may be some non-AIS proteins in our dataset owing to non-specific absorption of antibodies and signal amplification after biotinylation. Those contaminated biotinylated proteins reside in our inventory. Using ratiometric analysis against multiple reference controls, APL-AIS has certain resolution to dissect AIS enriched proteins, like AnkG, βIV-spectrin, NFASC, Nav1.2 and TRIM46 from others (Figure 2; Figure 3). The dispersed distribution of other AIS proteins might be attributed to their wide expression in neurons, relatively varied protein abundance at the AIS, and differences of

labeling efficiency. Screening these top ranked candidates by CRISPR-mediated endogenous gene tagging will be of considerable interest for future studies.

AIS composition may change substantially during neuronal development. For example, recent studies revealed that NuMA1 and P2Y1 participate only in AIS assembly [25,47]. Here, we applied TMT-based quantitative mass spectrometry to identify changes in the landscape of the AIS proteome, revealing a gradual increase of most AIS molecules, including the known AIS proteins βIV-spectrin, AnkG, NFASC and voltage-gated ion channels; these observations are consistent with previous analyses of AIS development using immunostaining methods [33]. While as many as 83.5% of proteins identified exhibited the highest level of enrichment at DIV21, we observed a few proteins that deviated from this general trend. For example, enrichment of the AIS protein TRIM46 reached its maximum at DIV7. This observation is in accordance with the proposed role of TRIM46 in establishing early neuronal polarity and axon specification [13].

Our dataset also revealed several highly enriched proteins that we subsequently confirmed may be located at the AIS, including SCRIB (ranked 8) and PHGDH (ranked 25). SCRIB has been reported to regulate synaptic plasticity, neurogenesis, neuronal migration and axonal connectivity [41-43]. We verified that SCRIB was highly expressed in the AIS both in cultured primary neurons and in brain slices. Since SCRIB is known to directly interact with β-spectrins in cell lines [48], its enrichment in the AIS might be due to binding with βIV-spectrin, which is in turn recruited by AIS master protein AnkG [49,50]. Additionally, super-resolution microscopy of SCRIB at AIS revealed a 189.4 ± 6.6 nm periodic distribution pattern that is reminiscent of βIV-spectrin's distribution. Further studies are needed to determine if SCRIB regulates aspects of AIS structure and function.

Another key finding is the discovery of PHGDH as a new AIS protein. As an enzyme involved in the serine biosynthesis pathway, PHGDH is traditionally considered to mainly function in neuroepithelium, radial glia cells and astrocytes [51]. To the best of our knowledge, no functional study of PHGDH has been reported in neurons. Here we confirmed its AIS

localization by 1) immunostaining, 2) detergent resistance, 3) smFP-V5 tagging of endogenous PHGDH using CRISPR, and 4) periodicity like that of other AIS proteins. Importantly, inhibition of neuronal PHGDH activity was essential for AIS integrity. Pharmacological inhibition of PHGDH reduced the density of AIS proteins, shortened AIS length, and decreased neuronal excitability. The identification of PHGDH highlights the utility of APL-AIS on profiling low expression but highly enriched proteins in the AIS [52]. Given calcium-dependent or cytoskeleton-dependent AIS regulation leads to changes on AIS components, length and position [3,5,53-56], it will be of interest to illustrate whether PHGDH effects on AIS is through direct interaction with AIS proteins or cytoskeleton, or indirect modulation by calcium-dependent mechanisms or PHGDH metabolic ways.

PHGDH deficiency in patients has been implicated with severe neurological symptoms including intractable seizures, psychomotor retardation and congenital microcephaly [36,57]. Abnormal expression of PHGDH has also been reported in mesial temporal lobe epilepsy with hippocampal sclerosis and Alzheimer' disease [58-60]. Whether neuronal PHGDH contributes to these neurological deficiencies is unknown. Future studies of PHGDH function *in vivo* will be of considerable interest and may provide clues to the pathogenesis of these PHGDH-related diseases.

Altogether, our study highlights the power of APL-AIS to discover novel AIS enriched proteins that regulate AIS structure and function. Much work remains to determine if other top ranked proteins also function at the AIS.

ACKNOWLEDGMENTS

We thank Y. Li, G. Wang, F. Yuan and Y. Chen for helpful discussions. This work was supported by the Ministry of Science and Technology (2018YFA0507600, 2017YFA0503600), the National Natural Science Foundation of China (32088101, 21727806). P.Z. is sponsored by Bayer Investigator Award. W.Z. was supported in part by the Postdoctoral Fellowship of Peking-Tsinghua Center for Life Sciences. We thank the

Analytical Instrumentation Center in Peking University for assistance with MS sample identification and Ms. W. Zhou for help with MS results analysis.

AUTHOR CONTRIBUTIONS

P.Z. and W.Z. conceived the project. W.Z., P.Z. and M.N.R. designed experiments. W.Z., Y.F., L.P., Y.O. and X.Z. performed experiments. W.Z. and P.Z. analyzed the data and wrote the paper with input from all authors. W.Z., P.Z. and M.N.R. revised the paper.

DATA AND MATERIALS AVAILABILITY

Requests for data, resources, and reagents should be directed to and will be fulfilled by the corresponding author, Dr. Peng Zou (zoupeng@pku.edu.cn).

DECLARATION OF INTERESTS

The authors declare no competing interests.

TEXT REFERENCES

1. Eichel, K., and Shen, K. (2022). The function of the axon initial segment in neuronal polarity. Developmental biology *489*, 47-54. 10.1016/j.ydbio.2022.05.016.

2. Kole, M.H., and Stuart, G.J. (2012). Signal processing in the axon initial segment. Neuron *73*, 235-247. 10.1016/j.neuron.2012.01.007.

3. Grubb, M.S., and Burrone, J. (2010). Activity-dependent relocation of the axon initial segment fine-tunes neuronal excitability. Nature *465*, 1070-1074. 10.1038/nature09160.

4. Kaphzan, H., Buffington, S.A., Jung, J.I., Rasband, M.N., and Klann, E. (2011). Alterations in intrinsic membrane properties and the axon initial segment in a mouse model of Angelman syndrome. The Journal of neuroscience : the official journal of the Society for Neuroscience *31*, 17637-17648. 10.1523/jneurosci.4162-11.2011.

5. Zhang, W., Ciorraga, M., Mendez, P., Retana, D., Boumedine-Guignon, N., Achón, B., Russier, M., Debanne, D., and Garrido, J.J. (2021). Formin Activity and mDia1 Contribute to Maintain Axon Initial Segment Composition and Structure. Molecular neurobiology *58*, 6153-6169. 10.1007/s12035-021-02531-6.

6. Hedstrom, K.L., Ogawa, Y., and Rasband, M.N. (2008). AnkyrinG is required for maintenance of the axon initial segment and neuronal polarity. The Journal of cell biology *183*, 635-640. 10.1083/jcb.200806112.

7. Sobotzik, J.M., Sie, J.M., Politi, C., Del Turco, D., Bennett, V., Deller, T., and Schultz, C. (2009). AnkyrinG is required to maintain axo-dendritic polarity in vivo. Proceedings of the National Academy of Sciences of the United States of America *106*, 17564-17569. 10.1073/pnas.0909267106.

8. Huang, C.Y., and Rasband, M.N. (2018). Axon initial segments: structure, function, and disease. Annals of the New York Academy of Sciences *1420*, 46-61. 10.1111/nyas.13718.

9. Kaphzan, H., Buffington, S.A., Ramaraj, A.B., Lingrel, J.B., Rasband, M.N., Santini, E., and Klann, E. (2013). Genetic reduction of the α1 subunit of Na/K-ATPase corrects multiple hippocampal phenotypes in Angelman syndrome. Cell reports *4*, 405-412. 10.1016/j.celrep.2013.07.005.

10. Sun, X., Wu, Y., Gu, M., Liu, Z., Ma, Y., Li, J., and Zhang, Y. (2014). Selective filtering defect at the axon initial segment in Alzheimer's disease mouse models. Proceedings of the National Academy of Sciences of the United States of America *111*, 14271-14276. 10.1073/pnas.1411837111.

11. Leterrier, C., Vacher, H., Fache, M.P., d'Ortoli, S.A., Castets, F., Autillo-Touati, A., and Dargent, B. (2011). End-binding proteins EB3 and EB1 link microtubules to ankyrin G in the axon initial segment. Proceedings of the National Academy of Sciences of the United States of America *108*, 8826-8831. 10.1073/pnas.1018671108.

12. Harterink, M., Vocking, K., Pan, X., Soriano Jerez, E.M., Slenders, L., Fréal, A., Tas, R.P., van de Wetering, W.J., Timmer, K., Motshagen, J., et al. (2019). TRIM46 Organizes Microtubule Fasciculation in the Axon Initial Segment. The Journal of neuroscience : the official journal of the Society for Neuroscience *39*, 4864-4873. 10.1523/jneurosci.3105-18.2019.

13. van Beuningen, S.F.B., Will, L., Harterink, M., Chazeau, A., van Battum, E.Y., Frias, C.P., Franker, M.A.M., Katrukha, E.A., Stucchi, R., Vocking, K., et al. (2015). TRIM46 Controls Neuronal Polarity and Axon Specification by Driving the Formation of Parallel Microtubule Arrays. Neuron *88*, 1208-1226. 10.1016/j.neuron.2015.11.012.

14. Bender, K.J., and Trussell, L.O. (2012). The physiology of the axon initial segment. Annual review of neuroscience *35*, 249-265. 10.1146/annurev-neuro-062111-150339.

15. Hedstrom, K.L., Xu, X., Ogawa, Y., Frischknecht, R., Seidenbecher, C.I., Shrager, P., and Rasband, M.N. (2007). Neurofascin assembles a specialized extracellular matrix at the axon initial segment. The Journal of cell biology *178*, 875-886. 10.1083/jcb.200705119.

16. Leterrier, C. (2016). The Axon Initial Segment, 50Years Later: A Nexus for Neuronal Organization and Function. Current topics in membranes *77*, 185-233. 10.1016/bs.ctm.2015.10.005.

17. Hamdan, H., Lim, B.C., Torii, T., Joshi, A., Konning, M., Smith, C., Palmer, D.J., Ng, P., Leterrier, C., Oses-Prieto, J.A., et al. (2020). Mapping axon initial segment structure and function by multiplexed proximity biotinylation. Nature communications *11*, 100. 10.1038/s41467-019-13658-5.

18. Chen, Y., Zhang, Y., Wang, Y., Zhang, L., Brinkman, E.K., Adam, S.A., Goldman, R., van Steensel, B., Ma, J., and Belmont, A.S. (2018). Mapping 3D genome organization relative to nuclear compartments using TSA-Seq as a cytological ruler. The Journal of cell biology *217*, 4025-4048. 10.1083/jcb.201807108.

19. Bar, D.Z., Atkatsh, K., Tavarez, U., Erdos, M.R., Gruenbaum, Y., and Collins, F.S. (2018). Biotinylation by antibody recognition-a method for proximity labeling. Nature methods *15*, 127-133. 10.1038/nmeth.4533.

20. Dopie, J., Sweredoski, M.J., Moradian, A., and Belmont, A.S. (2020). Tyramide signal amplification mass spectrometry (TSA-MS) ratio identifies nuclear speckle proteins. The Journal of cell biology *219*. 10.1083/jcb.201910207.

21. Li, X., Zhou, J., Zhao, W., Wen, Q., Wang, W., Peng, H., Gao, Y., Bouchonville, K.J., Offer, S.M., Chan, K., et al. (2022). Defining Proximity Proteome of Histone Modifications by Antibody-mediated Protein A-APEX2 Labeling. Genomics, proteomics & bioinformatics *20*, 87-100. 10.1016/j.gpb.2021.09.003.

22. Hung, V., Zou, P., Rhee, H.W., Udeshi, N.D., Cracan, V., Svinkina, T., Carr, S.A., Mootha, V.K., and Ting, A.Y. (2014). Proteomic mapping of the human mitochondrial intermembrane space in live cells via ratiometric APEX tagging. Molecular cell *55*, 332-341. 10.1016/j.molcel.2014.06.003.

23. Loh, K.H., Stawski, P.S., Draycott, A.S., Udeshi, N.D., Lehrman, E.K., Wilton, D.K., Svinkina, T., Deerinck, T.J., Ellisman, M.H., Stevens, B., et al. (2016). Proteomic Analysis of Unbounded Cellular Compartments: Synaptic Clefts. Cell *166*, 1295-1307.e1221. 10.1016/j.cell.2016.07.041.

24. Fréal, A., Rai, D., Tas, R.P., Pan, X., Katrukha, E.A., van de Willige, D., Stucchi, R., Aher, A., Yang, C., Altelaar, A.F.M., et al. (2019). Feedback-Driven Assembly of the Axon Initial Segment. Neuron *104*, 305-321.e308. 10.1016/j.neuron.2019.07.029.

25. Torii, T., Ogawa, Y., Liu, C.H., Ho, T.S., Hamdan, H., Wang, C.C., Oses-Prieto, J.A., Burlingame, A.L., and Rasband, M.N. (2020). NuMA1 promotes axon initial segment assembly through inhibition of endocytosis. The Journal of cell biology *219*. 10.1083/jcb.201907048.

26. Ke, M., Yuan, X., He, A., Yu, P., Chen, W., Shi, Y., Hunter, T., Zou, P., and Tian, R. (2021). Spatiotemporal profiling of cytosolic signaling complexes in living cells by selective proximity proteomics. Nature communications *12*, 71. 10.1038/s41467-020-20367-x.

27. Zhou, Y., Wang, G., Wang, P., Li, Z., Yue, T., Wang, J., and Zou, P. (2019). Expanding APEX2 Substrates for Proximity-Dependent Labeling of Nucleic Acids and Proteins in Living Cells. Angewandte Chemie (International ed. in English) *58*, 11763-11767. 10.1002/anie.201905949.

28. Lind, D., Franken, S., Kappler, J., Jankowski, J., and Schilling, K. (2005). Characterization of the neuronal marker NeuN as a multiply phosphorylated antigen with discrete subcellular localization. Journal of neuroscience research *79*, 295-302. 10.1002/jnr.20354.

29. Wolf, H.K., Buslei, R., Schmidt-Kastner, R., Schmidt-Kastner, P.K., Pietsch, T., Wiestler, O.D., and Blümcke, I. (1996). NeuN: a useful neuronal marker for diagnostic histopathology. The journal of histochemistry and cytochemistry : official journal of the Histochemistry Society *44*, 1167-1171. 10.1177/44.10.8813082.

30. Dehmelt, L., and Halpain, S. (2005). The MAP2/Tau family of microtubule-associated proteins. Genome biology *6*, 204. 10.1186/gb-2004-6-1-204.

31. Thompson, A., Schäfer, J., Kuhn, K., Kienle, S., Schwarz, J., Schmidt, G., Neumann, T., Johnstone, R., Mohammed, A.K., and Hamon, C. (2003). Tandem mass tags: a novel quantification strategy for comparative analysis of complex protein mixtures by MS/MS. Analytical chemistry *75*, 1895-1904. 10.1021/ac0262560.

32. Eichel, K., Uenaka, T., Belapurkar, V., Lu, R., Cheng, S., Pak, J.S., Taylor, C.A., Südhof, T.C., Malenka, R., Wernig, M., et al. (2022). Endocytosis in the axon initial segment maintains neuronal polarity. Nature *609*, 128-135. 10.1038/s41586-022-05074-5.

33. Jones, S.L., Korobova, F., and Svitkina, T. (2014). Axon initial segment cytoskeleton comprises a multiprotein submembranous coat containing sparse actin filaments. The Journal of cell biology *205*, 67-81. 10.1083/jcb.201401045.

34. Bas Orth, C., Schultz, C., Müller, C.M., Frotscher, M., and Deller, T. (2007). Loss of the cisternal organelle in the axon initial segment of cortical neurons in synaptopodin-deficient mice. The Journal of comparative neurology *504*, 441-449. 10.1002/cne.21445.

35. Ogawa, Y., Horresh, I., Trimmer, J.S., Bredt, D.S., Peles, E., and Rasband, M.N. (2008). Postsynaptic density-93 clusters Kv1 channels at axon initial segments independently of Caspr2. The Journal of neuroscience : the official journal of the Society for Neuroscience *28*, 5731-5739. 10.1523/jneurosci.4431-07.2008.

36. Furuya, S. (2008). An essential role for de novo biosynthesis of L-serine in CNS development. Asia Pacific journal of clinical nutrition *17 Suppl 1*, 312-315.

37. Garrido, J.J., Giraud, P., Carlier, E., Fernandes, F., Moussif, A., Fache, M.P., Debanne, D., and Dargent, B. (2003). A targeting motif involved in sodium channel clustering at the axonal initial segment. Science (New York, N.Y.) *300*, 2091-2094. 10.1126/science.1085167.

38. Winckler, B., Forscher, P., and Mellman, I. (1999). A diffusion barrier maintains distribution of membrane proteins in polarized neurons. Nature *397*, 698-701. 10.1038/17806.

39. Leterrier, C., Potier, J., Caillol, G., Debarnot, C., Rueda Boroni, F., and Dargent, B. (2015). Nanoscale Architecture of the Axon Initial Segment Reveals an Organized and Robust Scaffold. Cell reports *13*, 2781-2793. 10.1016/j.celrep.2015.11.051.

40. Xu, K., Zhong, G., and Zhuang, X. (2013). Actin, spectrin, and associated proteins form a periodic cytoskeletal structure in axons. Science (New York, N.Y.) *339*, 452-456. 10.1126/science.1232251.

41. Ezan, J., Moreau, M.M., Mamo, T.M., Shimbo, M., Decroo, M., Richter, M., Peyroutou, R., Rachel, R., Tissir, F., de Anda, F.C., et al. (2021). Early loss of Scribble affects cortical development, interhemispheric connectivity and psychomotor activity. Scientific reports *11*, 9106. 10.1038/s41598-021-88147-1.

42. Moreau, M.M., Piguel, N., Papouin, T., Koehl, M., Durand, C.M., Rubio, M.E., Loll, F., Richard, E.M., Mazzocco, C., Racca, C., et al. (2010). The planar polarity protein Scribble1 is essential for neuronal plasticity and brain function. The Journal of neuroscience : the official journal of the Society for Neuroscience *30*, 9738-9752. 10.1523/jneurosci.6007-09.2010.

43. Roche, J.P., Packard, M.C., Moeckel-Cole, S., and Budnik, V. (2002). Regulation of synaptic plasticity and synaptic vesicle dynamics by the PDZ protein Scribble. The Journal of neuroscience : the official journal of the Society for Neuroscience *22*, 6471-6479. 10.1523/jneurosci.22-15-06471.2002.

44. Pacold, M.E., Brimacombe, K.R., Chan, S.H., Rohde, J.M., Lewis, C.A., Swier, L.J., Possemato, R., Chen, W.W., Sullivan, L.B., Fiske, B.P., et al. (2016). A PHGDH inhibitor reveals coordination of serine synthesis and one-carbon unit fate. Nature chemical biology *12*, 452-458. 10.1038/nchembio.2070.

45. Raines, L.N., Zhao, H., Wang, Y., Chen, H.Y., Gallart-Ayala, H., Hsueh, P.C., Cao, W., Koh, Y., Alamonte-Loya, A., Liu, P.S., et al. (2022). PERK is a critical metabolic hub for immunosuppressive function in macrophages. Nature immunology *23*, 431-445. 10.1038/s41590-022-01145-x.

46. Mullarky, E., Lucki, N.C., Beheshti Zavareh, R., Anglin, J.L., Gomes, A.P., Nicolay, B.N., Wong, J.C., Christen, S., Takahashi, H., Singh, P.K., et al. (2016). Identification of a small molecule inhibitor of 3-phosphoglycerate dehydrogenase to target serine biosynthesis in

cancers. Proceedings of the National Academy of Sciences of the United States of America *113*, 1778-1783. 10.1073/pnas.1521548113.

47. Zhang, W., Bonadiman, A., Ciorraga, M., Benitez, M.J., and Garrido, J.J. (2019). P2Y1 Purinergic Receptor Modulate Axon Initial Segment Initial Development. Frontiers in cellular neuroscience *13*, 152. 10.3389/fncel.2019.00152.

48. Boëda, B., and Etienne-Manneville, S. (2015). Spectrin binding motifs regulate Scribble cortical dynamics and polarity function. eLife *4*. 10.7554/eLife.04726.

49. Jenkins, S.M., and Bennett, V. (2001). Ankyrin-G coordinates assembly of the spectrin-based membrane skeleton, voltage-gated sodium channels, and L1 CAMs at Purkinje neuron initial segments. The Journal of cell biology *155*, 739-746. 10.1083/jcb.200109026.

50. Yang, Y., Ogawa, Y., Hedstrom, K.L., and Rasband, M.N. (2007). betaIV spectrin is recruited to axon initial segments and nodes of Ranvier by ankyrinG. The Journal of cell biology *176*, 509-519. 10.1083/jcb.200610128.

51. Yamasaki, M., Yamada, K., Furuya, S., Mitoma, J., Hirabayashi, Y., and Watanabe, M. (2001). 3-Phosphoglycerate dehydrogenase, a key enzyme for l-serine biosynthesis, is preferentially expressed in the radial glia/astrocyte lineage and olfactory ensheathing glia in the mouse brain. The Journal of neuroscience : the official journal of the Society for Neuroscience *21*, 7691-7704. 10.1523/jneurosci.21-19-07691.2001.

52. Shimizu, M., Furuya, S., Shinoda, Y., Mitoma, J., Okamura, T., Miyoshi, I., Kasai, N., Hirabayashi, Y., and Suzuki, Y. (2004). Functional analysis of mouse 3-phosphoglycerate dehydrogenase (Phgdh) gene promoter in developing brain. Journal of neuroscience research *76*, 623-632. 10.1002/jnr.20102.

53. Berger, S.L., Leo-Macias, A., Yuen, S., Khatri, L., Pfennig, S., Zhang, Y., Agullo-Pascual, E., Caillol, G., Zhu, M.S., Rothenberg, E., et al. (2018). Localized Myosin II Activity Regulates Assembly and Plasticity of the Axon Initial Segment. Neuron *97*, 555-570.e556. 10.1016/j.neuron.2017.12.039.

54. Del Puerto, A., Fronzaroli-Molinieres, L., Perez-Alvarez, M.J., Giraud, P., Carlier, E., Wandosell, F., Debanne, D., and Garrido, J.J. (2015). ATP-P2X7 Receptor Modulates Axon Initial Segment Composition and Function in Physiological Conditions and Brain Injury. Cerebral cortex (New York, N.Y. : 1991) *25*, 2282-2294. 10.1093/cercor/bhu035.

55. Evans, M.D., Dumitrescu, A.S., Kruijssen, D.L.H., Taylor, S.E., and Grubb, M.S. (2015). Rapid Modulation of Axon Initial Segment Length Influences Repetitive Spike Firing. Cell reports *13*, 1233-1245. 10.1016/j.celrep.2015.09.066.

56. Jahan, I., Adachi, R., Egawa, R., Nomura, H., and Kuba, H. (2022). CDK5/p35-dependent microtubule reorganization contributes to homeostatic shortening of the axon initial

segment. JN-RM-0917-0922. 10.1523/JNEUROSCI.0917-22.2022 %J The Journal of Neuroscience.

57. Brassier, A., Valayannopoulos, V., Bahi-Buisson, N., Wiame, E., Hubert, L., Boddaert, N., Kaminska, A., Habarou, F., Desguerre, I., Van Schaftingen, E., et al. (2016). Two new cases of serine deficiency disorders treated with l-serine. European journal of paediatric neurology : EJPN : official journal of the European Paediatric Neurology Society *20*, 53-60. 10.1016/j.ejpn.2015.10.007.

58. Chen, X., Calandrelli, R., Girardini, J., Yan, Z., Tan, Z., Xu, X., Hiniker, A., and Zhong, S. (2022). PHGDH expression increases with progression of Alzheimer's disease pathology and symptoms. Cell metabolism *34*, 651-653. 10.1016/j.cmet.2022.02.008.

59. Furukawa, A., Kakita, A., Chiba, Y., Kitaura, H., Fujii, Y., Fukuda, M., Kameyama, S., and Shimada, A. (2020). Proteomic profile differentiating between mesial temporal lobe epilepsy with and without hippocampal sclerosis. Epilepsy research *168*, 106502. 10.1016/j.eplepsyres.2020.106502.

60. Le Douce, J., Maugard, M., Veran, J., Matos, M., Jégo, P., Vigneron, P.A., Faivre, E., Toussay, X., Vandenberghe, M., Balbastre, Y., et al. (2020). Impairment of Glycolysis-Derived l-Serine Production in Astrocytes Contributes to Cognitive Deficits in Alzheimer's Disease. Cell metabolism *31*, 503-517.e508. 10.1016/j.cmet.2020.02.004.

FIGURES

Figure 1

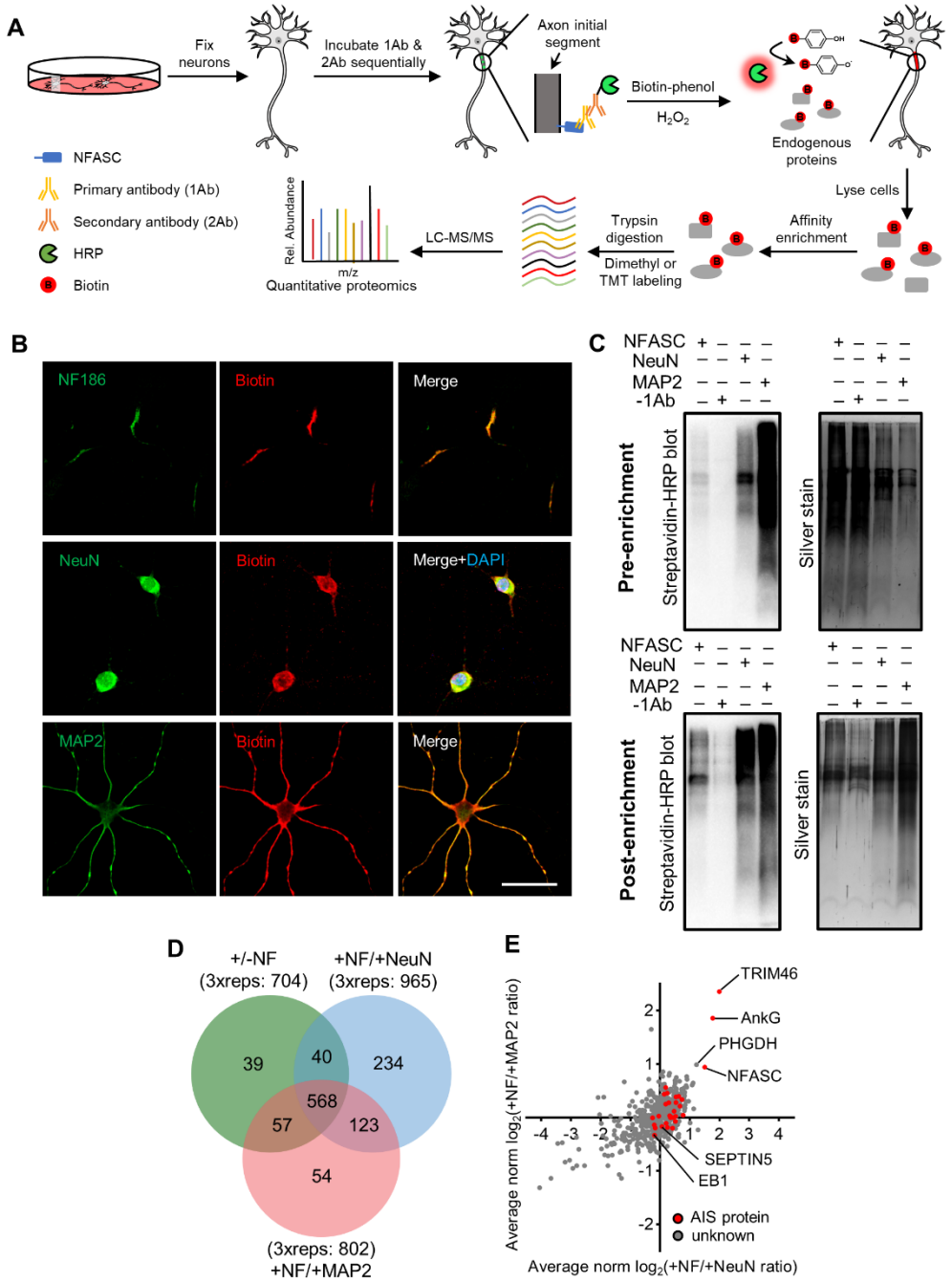

Figure 1. Development and validation of APL-AIS method.

(A) Experimental scheme of APL-AIS method. HRP is targeted to the axon initial segment in fixed cortical neurons through the specificity binding of anti-NFASC antibody (1Ab) and HRP conjugated second antibody (2Ab). HRP-mediated proximity biotinylation is triggered with the addition of biotin-phenol substrates and hydrogen peroxide. Biotinylated proteins are enriched via affinity purification, digested with trypsin, and identified via LC-MS/MS analysis.

(B) Representative images of biotinylated proteins colocalize with endogenous proteins signal in the axon initial segment, soma and somatodendrites. The proximity labeling was targeted by anti-NFASC, anti-NeuN and anti-MAP2 antibodies individually in DIV14 cortical neurons. Bar= 50 μm.

(C) Streptavidin blots and silver staining of DIV12 cortical neuron lysates (pre-enrichment) or streptavidin bead elute (post-enrichment) in conditions of anti-NFASC, no primary antibody (-1Ab), anti-NeuN and anti-MAP2 targeted proximity labeling. Samples of anti-NFASC, -1Ab, anti-NeuN and anti-MAP2 were loaded as the ratio of 4:4:2:1.

(D) Venn diagrams showing 568 overlapped biotinylated proteins from +NFASC/+NeuN, +NFASC/+MAP2 and filtered +/-NFASC datasheet. Three times independent dimethyl proteome replicates were performed in each condition.

(E) Scatterplot showing the enrichment of anti-NFASC captured biotinylated proteins over soma (x-axis) and somatodendrites (y-axis) intensity in the reference of average normalized $\log_2$(H/L ratios). Red dots indicate reported AIS components and gray dots are proteins having no AIS information.

Figure 2

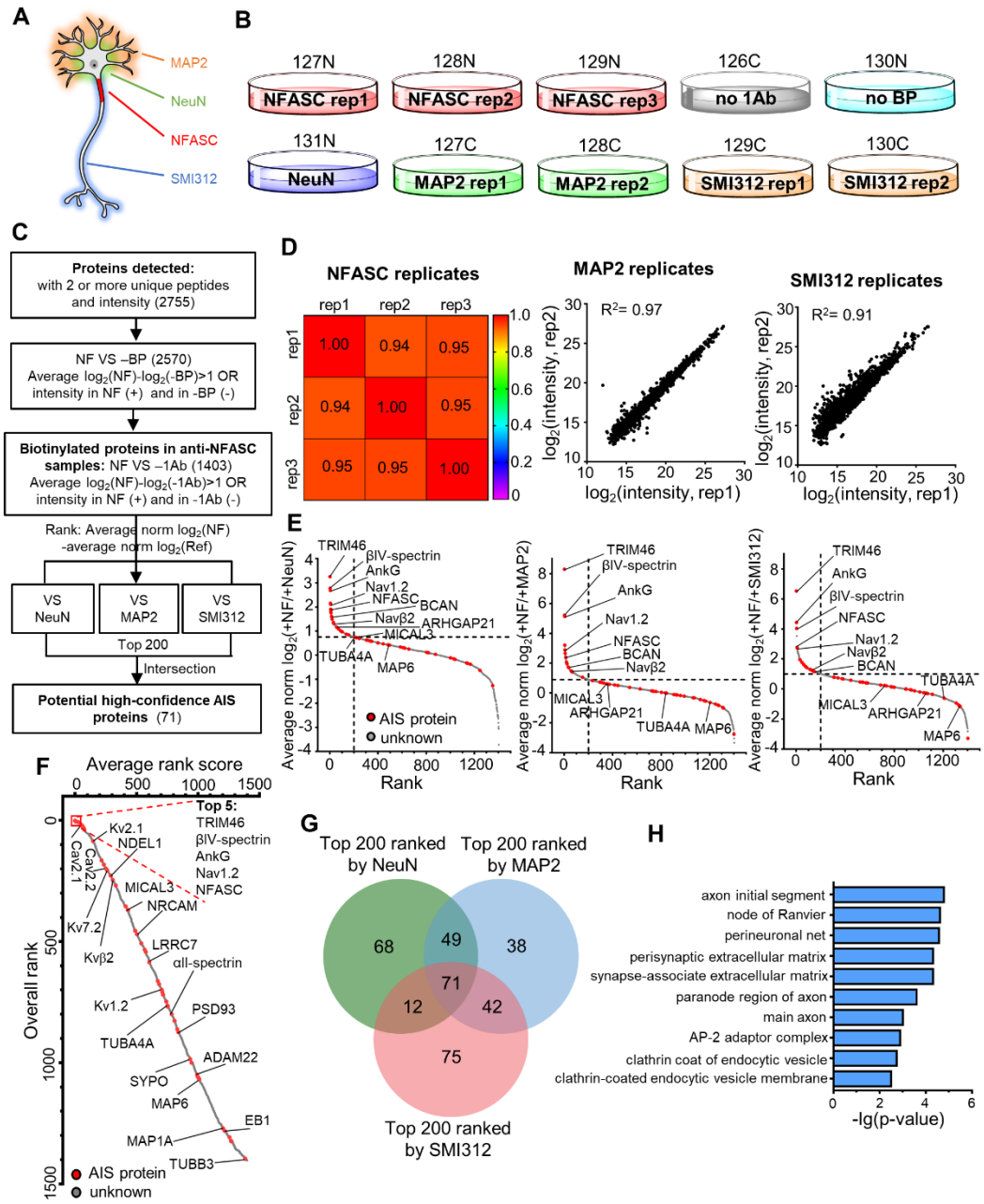
A
MAP2
NeuN
NFASC
SMI312
B
127N
128N
129N
126C
130N
NFASC rep1
NFASC rep2
NFASC rep3
no 1Ab
no BP
131N
127C
128C
129C
130C
NeuN
MAP2 rep1
MAP2 rep2
SMI312 rep1
SMI312 rep2
C
Proteins detected: with 2 or more unique peptides and intensity (2755)
NF VS –BP (2570) Average log2(NF)-log2(-BP)>1 OR intensity in NF (+) and in -BP (-)
Biotinylated proteins in anti-NFASC samples: NF VS –1Ab (1403) Average log2(NF)-log2(-1Ab)>1 OR intensity in NF (+) and in -1Ab (-)
Rank: Average norm log2(NF) -average norm log2(Ref)
VS NeuN
VS MAP2
VS SMI312
Top 200
Intersection
Potential high-confidence AIS proteins (71)
D
NFASC replicates
MAP2 replicates
SMI312 replicates
rep1
rep2
rep3
1.00
0.94
0.95
R2= 0.97
R2= 0.91
log2(intensity, rep2)
log2(intensity, rep1)
E
Average norm log2(+NF/+NeuN)
Average norm log2(+NF/+MAP2)
Average norm log2(+NF/+SMI312)
Rank
TRIM46
βIV-spectrin
AnkG
Nav1.2
NFASC
BCAN
Navβ2
ARHGAP21
MICAL3
TUBA4A
MAP6
AIS protein
unknown
F
Average rank score
Overall rank
Top 5:
TRIM46
βIV-spectrin
AnkG
Nav1.2
NFASC
Kv2.1
NDEL1
Cav2.1
Cav2.2
MICAL3
NRCAM
Kv7.2
Kvβ2
LRRC7
αII-spectrin
Kv1.2
PSD93
TUBA4A
ADAM22
SYPO
MAP6
EB1
MAP1A
TUBB3
AIS protein
unknown
G
Top 200 ranked by NeuN
Top 200 ranked by MAP2
Top 200 ranked by SMI312
68
49
38
71
12
42
75
H
axon initial segment
node of Ranvier
perineuronal net
perisynaptic extracellular matrix
synapse-associate extracellular matrix
paranode region of axon
main axon
AP-2 adaptor complex
clathrin coat of endocytic vesicle
clathrin-coated endocytic vesicle membrane
-lg(p-value)

Figure 2. Axon initial segment proteome profiling at DIV14.

(A) Schematic picture of neurons biotinylated in axon initial segment by targeting NFASC (red), soma by targeting NeuN (green), somatodendrites by targeting MAP2 (orange) and axon by targeting phosphorylated axonal neurofilaments using SMI312 antibody (blue).

(B) Design of 10-plex TMT for AIS quantitative proteomic experiments. Samples were collected from at least three independent cultural neurons. TMT tags were labelled on the dishes.

(C) Workflow for AIS proteomes analysis.

(D) Correlation analysis of biological replicates showing high reproducibility. Pearson correlation was applied to parallel analysis of 2377, 2691 and 2498 common elements in anti-NFASC, anti-MAP2 and anti-SMI312 replicates respectively.

(E) Ranking 1403 biotinylated proteins based on their averaged MS intensity ratios. Red dots indicate reported AIS components and gray dots are proteins having no AIS information.

(F) Overall rank plot integrating three references (E) listing potential AIS enriched proteins in top positions. Proteins are sorted by average rank scores from +NFASC/+NeuN, +NFASC/+MAP2 and +NFASC/+SMI312 experiments. Red dots indicate reported AIS components and gray dots are proteins having no AIS information. Some known AIS proteins are labelled in the graph.

(G) Venn diagrams showing 71 high-confidence AIS candidates from top 200 data of +NFASC/+NeuN, +NFASC/+MAP2 and +NFASC/+SMI312 experiments.

(H) Top 10 cellular compartment terms. 71 high-confidence AIS candidates were applied to Gene Oncology cellular compartment analysis. A total of 2744 valid proteins in this TMT were used as a reference (2755 proteins identified and 2744 valid data in Gene Oncology).

Figure 3

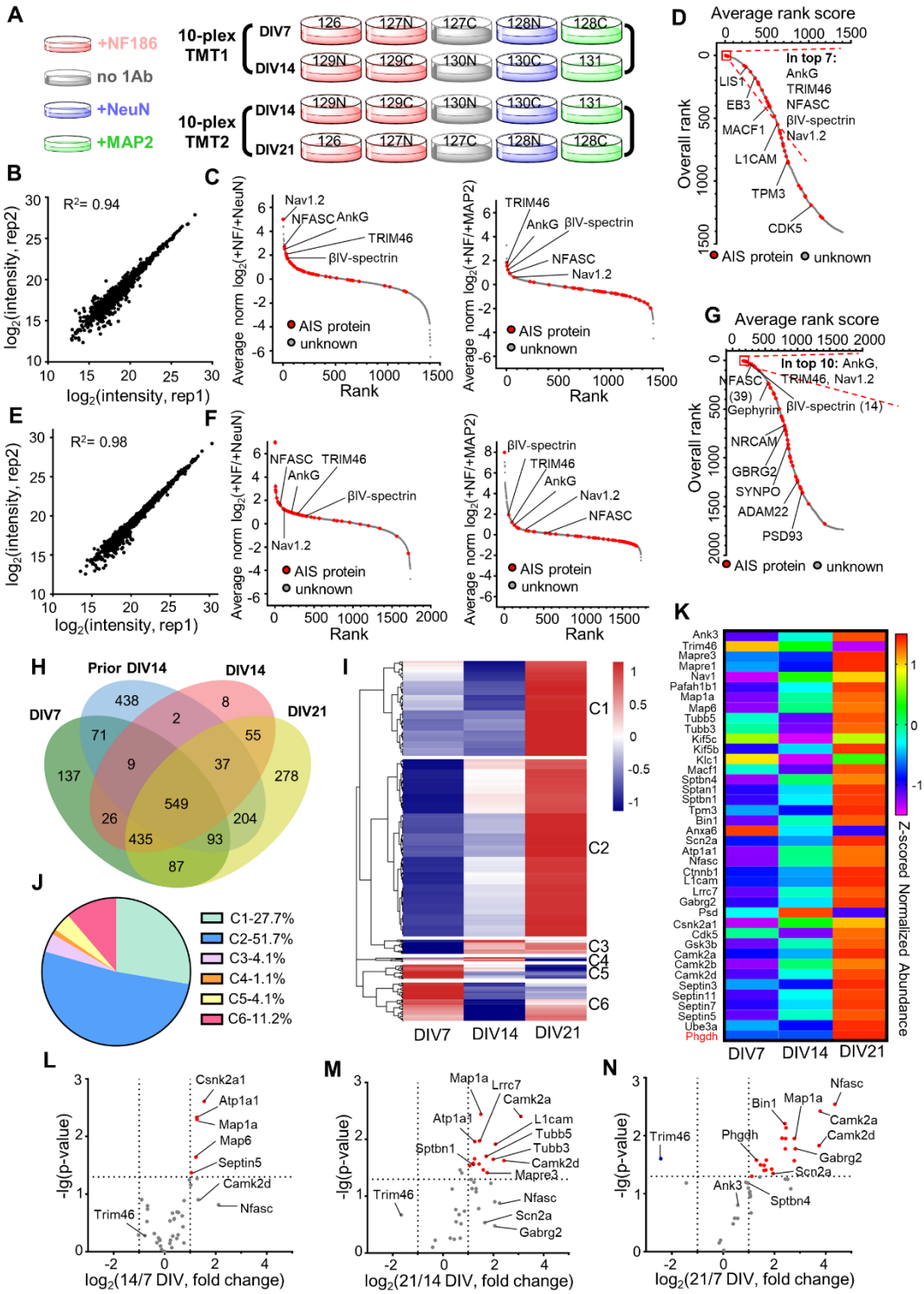
A
+NF186
no 1Ab
+NeuN
+MAP2
10-plex TMT1
DIV7
DIV14
126
127N
127C
128N
128C
129N
129C
130N
130C
131
10-plex TMT2
DIV14
DIV21
B
R²= 0.94
log2(intensity, rep2)
log2(intensity, rep1)
C
Nav1.2
NFASC
AnkG
TRIM46
βIV-spectrin
AIS protein
unknown
Average norm log2(+NF/+NeuN)
Rank
Average norm log2(+NF/+MAP2)
D
Average rank score
Overall rank
In top 7:
AnkG
TRIM46
NFASC
βIV-spectrin
Nav1.2
LIS1
EB3
MACF1
L1CAM
TPM3
CDK5
E
R²= 0.98
F
G
In top 10: AnkG, TRIM46, Nav1.2
NFASC (39)
βIV-spectrin (14)
Gephyrin
NRCAM
GBRG2
SYNPO
ADAM22
PSD93
H
Prior DIV14
DIV14
DIV7
DIV21
438
8
2
71
55
9
37
137
278
549
26
204
435
93
87
I
C1
C2
C3
C4
C5
C6
DIV7
DIV14
DIV21
J
C1-27.7%
C2-51.7%
C3-4.1%
C4-1.1%
C5-4.1%
C6-11.2%
K
Ank3
Trim46
Mapre3
Mapre1
Nav1
Pafah1b1
Map1a
Map6
Tubb5
Tubb3
Kif5c
Kif5b
Klc1
Macf1
Sptbn4
Sptan1
Sptbn1
Tpm3
Bin1
Anxa6
Scn2a
Atp1a1
Nfasc
Ctnnb1
L1cam
Lrrc7
Gabrg2
Psd
Csnk2a1
Cdk5
Gsk3b
Camk2a
Camk2b
Camk2d
Septin3
Septin11
Septin7
Septin5
Ube3a
Phgdh
Z-scored Normalized Abundance
L
Csnk2a1
Atp1a1
Map1a
Map6
Septin5
Camk2d
Nfasc
Trim46
-lg(p-value)
log2(14/7 DIV, fold change)
M
Map1a
Lrrc7
Camk2a
Atp1a3
L1cam
Tubb5
Tubb3
Sptbn1
Camk2d
Mapre3
Trim46
Nfasc
Scn2a
Gabrg2
log2(21/14 DIV, fold change)
N
Nfasc
Bin1
Map1a
Camk2a
Camk2d
Trim46
Phgdh
Gabrg2
Scn2a
Ank3
Sptbn4
log2(21/7 DIV, fold change)

Figure 3. Mapping axon initial segment developmental proteome.

(A) Design of AIS developmental proteome using two parallel 10-plex TMT: DIV7 for early AIS, DIV14 for mature AIS and DIV21 for completely mature AIS.

(B) Pearson correlation showing high reproducibility in anti-NFASC targeted AIS proximity labeling for DIV7 cortical neurons (1532 common elements from 2 replicates).

(C) Ranking DIV7 AIS biotinylated 1407 proteins according to their averaged MS intensity ratios (+NFASC/+NeuN and +NFASC/+MAP2).

(D) DIV7 overall rank plot listing potential AIS proteins. Proteins are sorted by the average rank scores from +NFASC/+NeuN and +NFASC/+MAP2 experiments (C). Some known AIS proteins are labelled in the graph. Red dots indicate reported AIS components and gray dots are proteins having no AIS information.

(E) Pearson correlation showing high reproducibility in anti-NFASC targeted AIS proximity labeling for DIV21 cortical neurons (1859 common elements from 2 replicates).

(F) Ranking DIV21 AIS biotinylated 1738 proteins according to their averaged MS intensity ratios (+NFASC/+NeuN and +NFASC/+MAP2).

(G) DIV21 overall rank plot listing potential AIS proteins. Proteins are sorted by the average rank scores from +NFASC/+NeuN and +NFASC/+MAP2 experiments (F). Some known AIS proteins are labelled in the graph. Red dots indicate reported AIS components and gray dots are proteins having no AIS information.

(H) Venn diagrams showing 549 common AIS candidates at DIV7, 14 and 21. Our prior AIS inventory of DIV14 was also utilized for the overlapping analysis.

(I) Six clusters with distinct protein expression profiles were generated by pheatmap analysis in R package along neuronal development.

(J) The percentage of protein numbers in each cluster in 534 analyzed proteins.

(K) AIS protein expression patterns along neuronal development. Red labelled protein PHGDH is a novel AIS enriched protein identified in this study. Proteins are represented by their gene names.

(L-N) Volcano plots showing AIS proteins fold changes between DIV7 and 14 (L), DIV 14 and 21 (M) or DIV7 and 21 (N). Red and blue points represent AIS proteins with significant up-regulation and down-regulation respectively. Proteins are represented by their gene names. Horizontal dashed lines indicate p= 0.05. Vertical dashed lines indicate the cutoff of $\log_2$(fold change) = ±1.

Figure 4

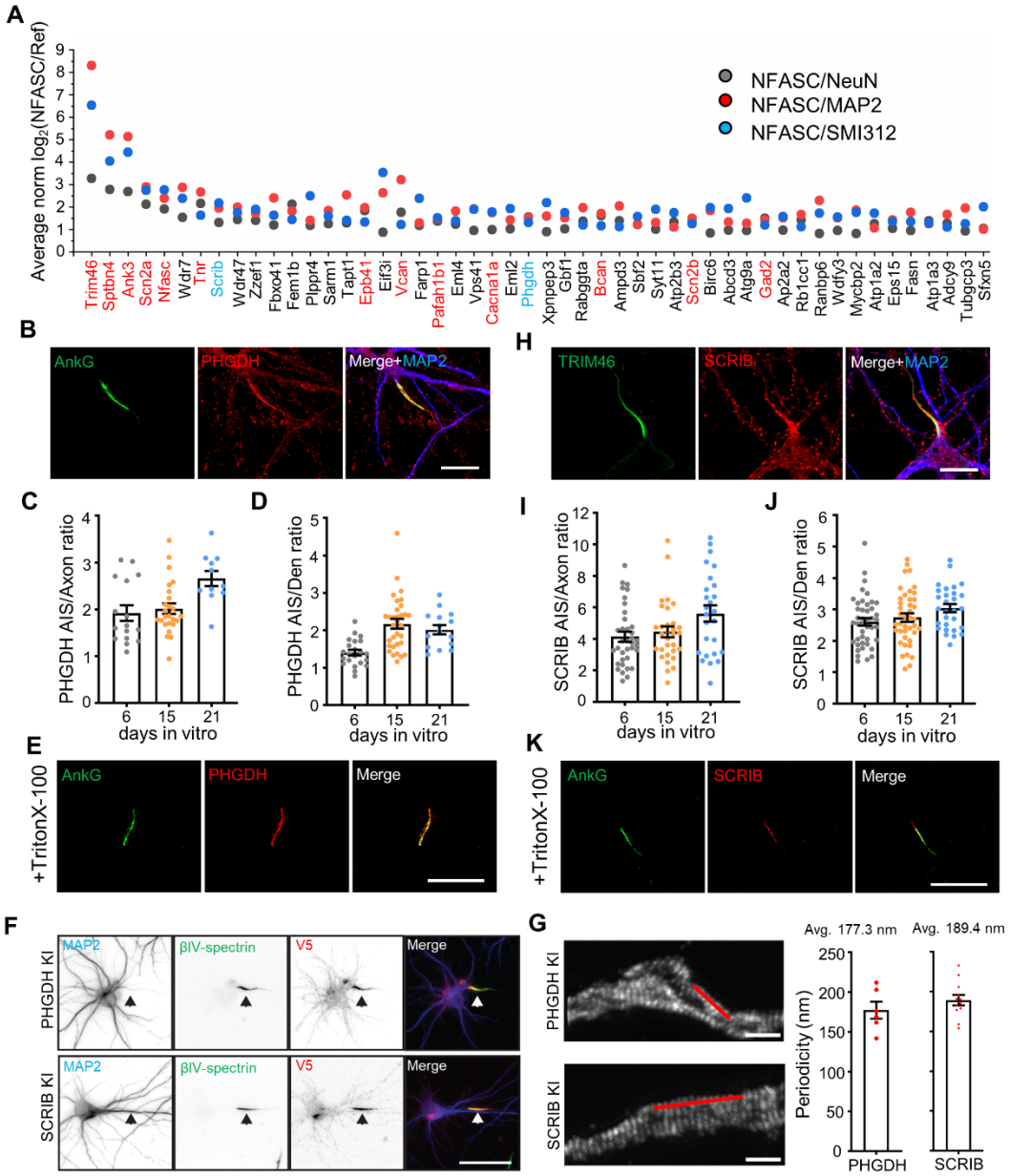
A
Average norm log2(NFASC/Ref)
NFASC/NeuN
NFASC/MAP2
NFASC/SMI312
Trim46 Sptbn4 Ank3 Scn2a Nfasc Wdr7 Tnr Scrib Wdr47 Zzef1 Fbxo41 Fem1b Plppr4 Sarm1 Tapt1 Epb41 Eif3i Vcan Farp1 Pafah1b1 Eml4 Vps41 Cacna1a Eml2 Phgdh Xpnpep3 Gbf1 Rabggta Bcan Ampd3 Sbf2 Syt11 Atp2b3 Scn2b Birc6 Abcd3 Atg9a Gad2 Ap2a2 Rb1cc1 Ranbp6 Wdfy3 Mycbp2 Atp1a2 Eps15 Fasn Atp1a3 Adcy9 Tubgcp3 Sfxn5
B
AnkG
PHGDH
Merge+MAP2
H
TRIM46
SCRIB
Merge+MAP2
C
PHGDH AIS/Axon ratio
days in vitro
D
PHGDH AIS/Den ratio
days in vitro
I
SCRIB AIS/Axon ratio
days in vitro
J
SCRIB AIS/Den ratio
days in vitro
E
+TritonX-100
AnkG
PHGDH
Merge
K
+TritonX-100
AnkG
SCRIB
Merge
F
PHGDH KI
SCRIB KI
MAP2
βIV-spectrin
V5
Merge
G
PHGDH KI
SCRIB KI
Avg. 177.3 nm
Avg. 189.4 nm
Periodicity (nm)
PHGDH
SCRIB

Figure 4. SCRIB and PHGDH polarize in the axon initial segment.

(A) Top 50 ranked AIS candidates in DIV14 AIS inventory list, showing fold changes of proteins intensity in the AIS against in soma, somatodendrites and the axon. Known AIS proteins are shown in red, validated novel AIS proteins in this study are shown in blue and the rest are unknown proteins. Proteins are represented by their gene names.

(B) Representative images of DIV15 cortical neurons stained with AnkG (green, AIS), PHGDH (red) and MAP2 (blue, somatodendrites) showing high expression of PHGDH in the AIS. Bar= 20 μm.

(C-D) Quantification of PHGDH mean intensity in the AIS versus in the axon (C, 40 μm away from the distal end of AIS) or in proximal dendrites (D) reveals polarized distribution of PHGDH in the AIS along neuronal development. Two times independent experiments were performed.

(E) Representative images of DIV12 cortical neurons showing a TritonX-100 detergent-resistant pool of PHGDH (red) at the AIS (green, AnkG). Bar= 20 μm.

(F) Representative images of smFP-V5 tag knock-in neurons to PHGDH and SCRIB. Cultured rat hippocampal neurons were infected with two AAVs, one is for Cas9 expression and another one is for gRNA and donor expression for homology-independent knock-in at DIV0. Neurons were fixed at DIV15 and stained with the indicated antibodies. Arrows indicate the position of AIS. Bar= 50 μm.

(G) Representative STED images of smFP-V5 tag knock-in neurons to PHGDH and SCRIB. Knock-in neurons were fixed at DIV21 for PHGDH and DIV16 for SCRIB, and stained with V5-tag antibody. Regions indicated by red lines were used to generate the intensity profiles, and the average periodicities were calculated. Error bars represent mean ± SEM. Bar= 1 μm.

(H) Representative images of DIV15 cortical neurons stained with TRIM46 (green, AIS), SCRIB (red) and MAP2 (blue, somatodendrites) showing high expression of SCRIB in the AIS. Bar= 20 μm.

(I-J) Quantification of SCRIB mean intensity in the AIS versus in the axon (I, 40 μm away from the distal end of AIS) or in proximal dendrites (J) reveals polarized distribution of SCRIB in the AIS along neuronal development. Two times independent experiments were performed.

(K) Representative images of DIV12 cortical neurons showing a TritonX-100 detergent-resistant pool of SCRIB (red) at the AIS (green, AnkG). Bar= 20 μm.

Figure 5

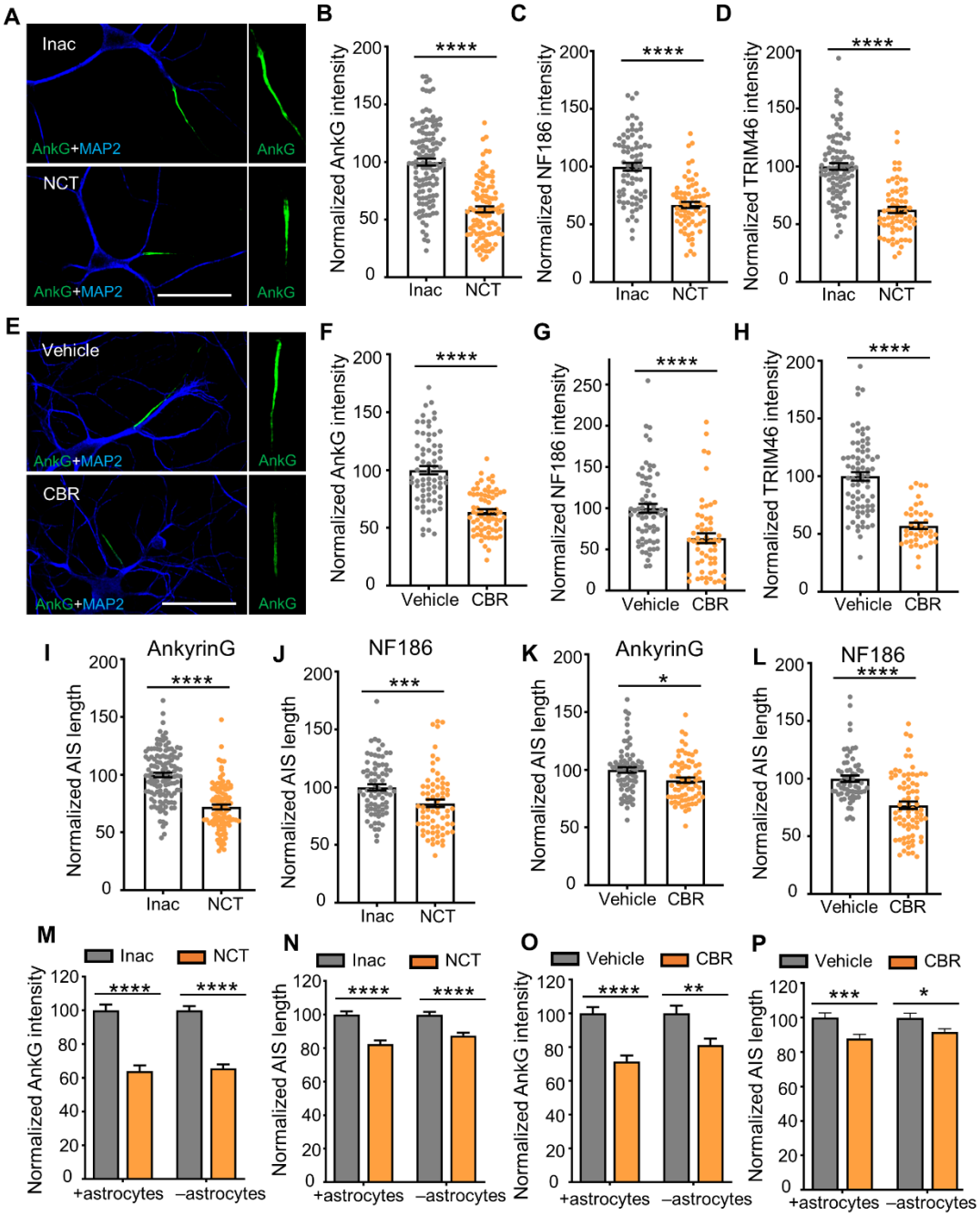
A
Inac
AnkG+MAP2
AnkG
NCT
AnkG+MAP2
AnkG
B
Normalized AnkG intensity
****
Inac
NCT
C
Normalized NF186 intensity
****
Inac
NCT
D
Normalized TRIM46 intensity
****
Inac
NCT
E
Vehicle
AnkG+MAP2
AnkG
CBR
AnkG+MAP2
AnkG
F
Normalized AnkG intensity
****
Vehicle
CBR
G
Normalized NF186 intensity
****
Vehicle
CBR
H
Normalized TRIM46 intensity
****
Vehicle
CBR
I
AnkyrinG
Normalized AIS length
****
Inac
NCT
J
NF186
***
Inac
NCT
K
AnkyrinG
*
Vehicle
CBR
L
NF186
****
Vehicle
CBR
M
Inac
NCT
Normalized AnkG intensity
****
****
+astrocytes
–astrocytes
N
Inac
NCT
Normalized AIS length
****
****
+astrocytes
–astrocytes
O
Vehicle
CBR
Normalized AnkG intensity
****
**
+astrocytes
–astrocytes
P
Vehicle
CBR
Normalized AIS length
***
*
+astrocytes
–astrocytes

Figure 5. PHGDH inhibition disrupts AIS structure.

(A) Representative images of DIV15 cortical neurons treated with 50 μM PHGDH inhibitor NCT503 or non-effective analogue Inac for 48 h. MAP2 labelling (blue) indicates healthy neuronal morphology with or without NCT503 treatment, while AnkG labelling (green) shows the AIS structural changes. Enlarged images of AnkG are presented in the right panel. Bar= 50 μm.

(B) PHGDH inhibition by NCT503 for 48 h significantly decreases AnkG intensity in the AIS. Quantification of integrated AnkG intensity from experiments (A). Three times independent experiments were performed. Graphs are presented as mean ± SEM. Mann-Whitney test, ****$p<0.0001$.

(C-D) PHGDH inhibition by 50 μM NCT503 for 48 h significantly decreases NF186 (C) and TRIM46 (D) intensity in the AIS. Two times independent experiments were performed. Graphs are presented as mean ± SEM. Unpaired t-test, ****$p<0.0001$.

(E) Representative images of DIV21 cortical neurons treated with 50 μM PHGDH inhibitor CBR5884 or vehicle DMSO for 48 h. MAP2 labelling (blue) indicates healthy neuronal morphology with or without CBR5884 treatment, while AnkG labelling (green) shows the AIS structural changes. Enlarged images of AnkG are presented in the right panel. Bar= 50 μm.

(F) PHGDH inhibition by CBR5884 for 48 h significantly decreases AnkG intensity in the AIS. Quantification of integrated AnkG intensity from experiments (E). Two times independent experiments were performed. Graphs are presented as mean ± SEM. Unpaired t-test, ****$p<0.0001$.

(G-H) PHGDH inhibition by 50 μM CBR5884 for 48 h significantly decreases NF186 (G) and TRIM46 (H) intensity in the AIS. Two times independent experiments were performed. Graphs are presented as mean ± SEM. Mann-Whitney test for NF186 statistical analysis and Unpaired t-test for TRIM46 statistical analysis, ****$p<0.0001$.

(I-J) PHGDH inhibition by NCT503 for 48 h treatment significantly shortens AIS length

evaluated by AnkG (I) and NF186 (J). At least two times independent experiments were performed. Graphs are presented as mean ± SEM. Mann-Whitney test, ****p<0.0001; ***p<0.001.

(K-L) PHGDH inhibition by CBR5884 for 48 h treatment significantly shortens AIS length evaluated by AnkG (K) and NF186 (L). Two times independent experiments were performed. Graphs are presented as mean ± SEM. Mann-Whitney test, ****p<0.0001; *p<0.05.

(M-N) The effects of PHGDH inhibitor NCT503 on AIS is independent of micro-environmental astrocytes. Cortical neurons were cultured with astrocytes as feeder layer. AraC was added after 1 day plating to curb glial cells proliferation. The neuronal treatment in conditioned medium is defined as '–astrocytes', while in the neuron-glia cultured system is defined as '+astrocytes'. Quantification of integrated AnkG intensity (M) and AIS length (N) in DIV14 cortical neurons after 48 h treatment with 50 μM NCT503 or Inac. Two times independent experiments were performed. Graphs are presented as mean ± SEM. Mann-Whitney test, ****p<0.0001.

(O-P) The effects of PHGDH inhibitor CBR5884 on AIS with or without astrocytes. Quantification of integrated AnkG intensity (O) and AIS length (P) in DIV12 cortical neurons after 3 h treatment with 50 μM CBR5884 or DMSO. Two times independent experiments were performed. Graphs are presented as mean ± SEM. Mann-Whitney test, ****p<0.0001; ***p<0.001; **p<0.01; *p<0.05.

Figure 6

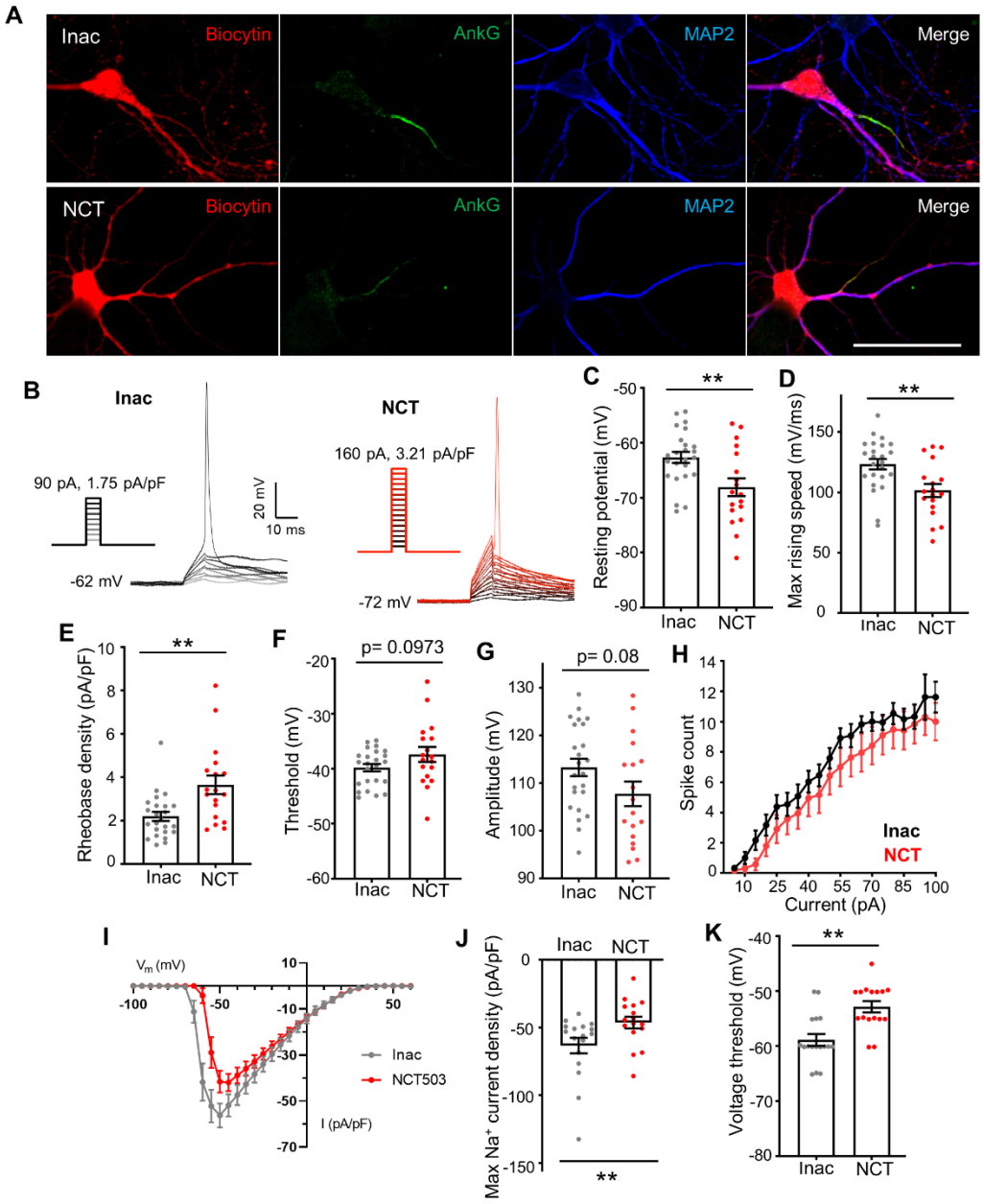
A
Inac
Biocytin
AnkG
MAP2
Merge
NCT
Biocytin
AnkG
MAP2
Merge
B
Inac
90 pA, 1.75 pA/pF
20 mV
10 ms
-62 mV
NCT
160 pA, 3.21 pA/pF
-72 mV
C
**
Resting potential (mV)
Inac
NCT
D
**
Max rising speed (mV/ms)
Inac
NCT
E
**
Rheobase density (pA/pF)
Inac
NCT
F
p= 0.0973
Threshold (mV)
Inac
NCT
G
p= 0.08
Amplitude (mV)
Inac
NCT
H
Spike count
Current (pA)
Inac
NCT
I
Vm (mV)
Inac
NCT503
I (pA/pF)
J
Inac
NCT
Max Na+ current density (pA/pF)
**
K
**
Voltage threshold (mV)
Inac
NCT

Figure 6. Losing PHGDH activity decreases neuronal intrinsic excitability.

(A) Representative patched neurons showing AIS structural changes after NCT503 treatment. DIV12 cortical neurons were treated with 50 μM NCT503 or non-effective analogue Inac for 48 h. Biocytin was injected to identify patched neurons. AIS structure is indicated by AnkG labelling (green). Bar= 50 μm.

(B) Representative current-clamp traces recorded from 10-ms-duration current injection steps (2.1 Hz) with increasing strength from 10 pA to 500 pA (increments of 10 pA). Numbers indicate the rheobase (pA), rheobase density (pA/pF) and resting membrane potential (mV).

(C-G) Quantification of resting potential (C), maximal rising speed (D), rheobase density (E), voltage threshold (F), and amplitude (G). D-G graphs were analyzed from the very first evoked action potential. Three times independent experiments were performed. Mann-Whitney test was used for rheobase density statistical analysis. Unpaired t-test was used for resting potential, maximal rising speed, threshold voltage, and amplitude statistical analysis. Data are represented as mean ± SEM, **$p<0.01$, Inac, n= 24; NCT503, n= 18.

(H) The number of evoked action potentials in 500-ms current injection was plotted against current injection steps (1 Hz) from 5 pA to 100 pA (increments of 5 pA). Three times independent experiments were performed. Multiple t tests were used for statistical analysis, Inac, n= 24; NCT503, n= 18.

(I-K) The current density-voltage curve of the voltage-gated sodium channel (I), maximal voltage-gated sodium channel current density of each cell (J) and the voltage threshold of the voltage-gated sodium channel (K) recorded in Inac or NCT503 treated neurons. Neurons were held at –80 mV and applied 500-ms-duration voltage change pulse steps (1 Hz) from -100 mV to 60 mV (increments of 5 mV). Data are represented as mean ± SEM. Two times independent experiments were performed. Mann-Whitney test was used for statistical analysis, with **$p<0.01$. Inac, n= 17; NCT503, n= 16.

Figure S1

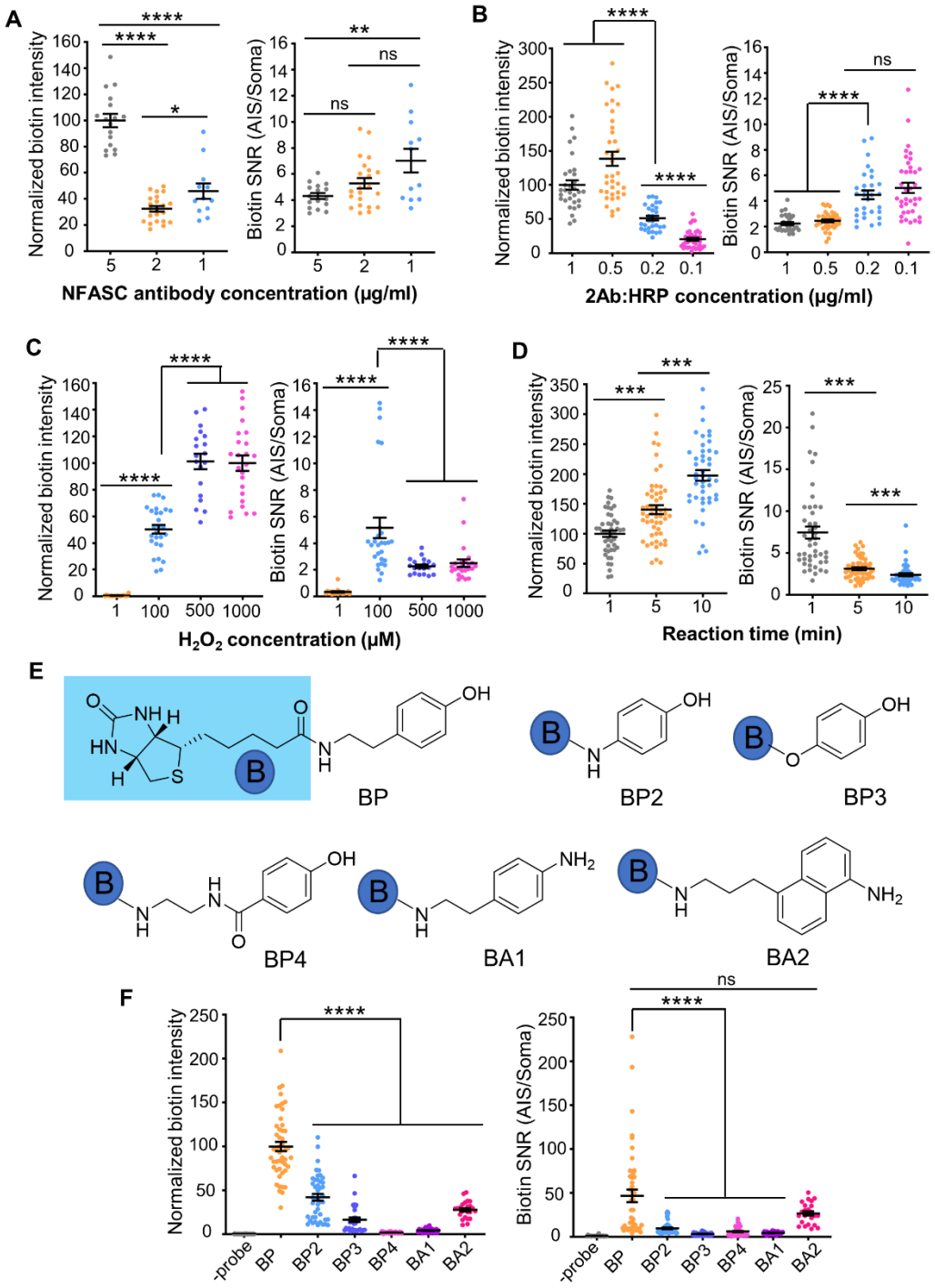
A
Normalized biotin intensity
Biotin SNR (AIS/Soma)
NFASC antibody concentration (μg/ml)
B
2Ab:HRP concentration (μg/ml)
C
H_2O_2 concentration (μM)
D
Reaction time (min)
E
BP
BP2
BP3
BP4
BA1
BA2
F
-probe
BP
BP2
BP3
BP4
BA1
BA2

Figure S1. Related to Figure 1. Optimization of anti-NFASC targeted AIS proximity labelling.

(A-F) Anti-NFASC antibody targeted AIS proximity labelling parameters were tested in DIV10-14 fixed cortical neurons. Tested parameters are as follows: first antibody (1Ab, A), HRP conjugated second antibody (2Ab, B) and H_2O_2 concentration (C), reaction duration (D) and reaction substrates (F). The stock concentration of 1Ab and 2Ab is 1 mg/ml. (E) Chemical probes tested in this study. Experiments were performed with single variable only. The labelling efficiency is evaluated by the mean intensity of biotinylated proteins signal in the AIS. The labelling specificity is evaluated by the ratio of biotinylated proteins signal in the AIS to that in the soma (SNR). At least two independent experiments were performed. Graphs are presented as mean ± SEM, ****$p<0.0001$; ***$p<0.001$; **$p<0.01$; *$p<0.05$ and ns, not significant.

Figure S2

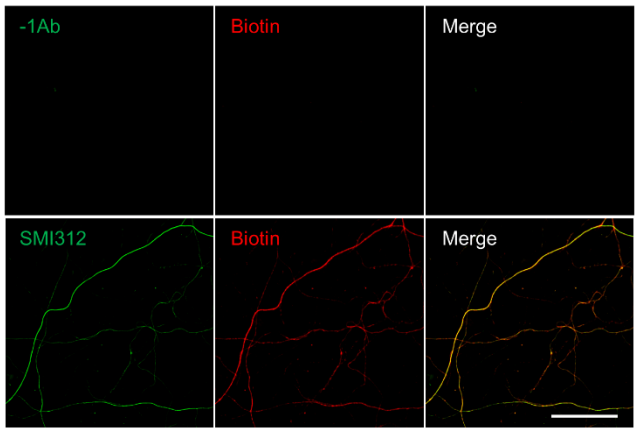

Figure S2. Related to Figure 2. Specificity verification of SMI312 targeted axon proximity labeling. Fixed DIV14 cortical neurons were processed for proximity labeling with or without SMI312 antibody. Biotinylated proteins signal is in red, endogenous proteins signal labelled by SMI312 is in green. Bar= 50 μm.

Figure S3

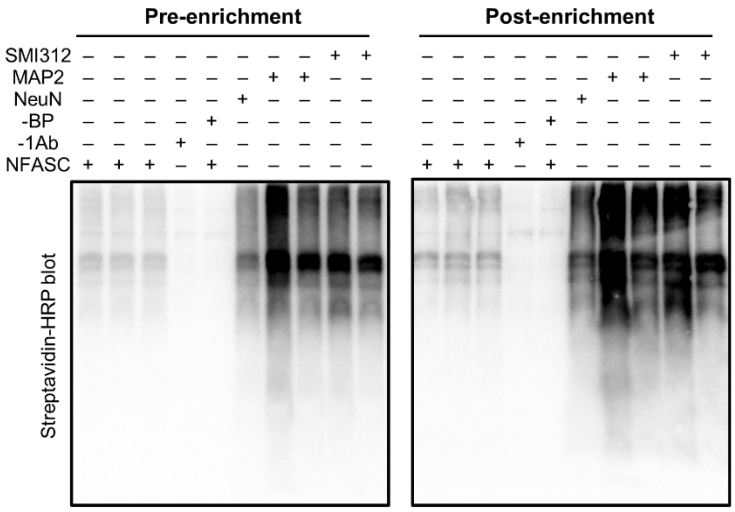

Figure S3. Related to Figure 2. Proximity labeling and enrichment test in DIV14 TMT experiments. Streptavidin blots of DIV14 cortical neuron lysates (pre-enrichment) or streptavidin bead elute (post-enrichment) from samples of anti-NFASC, NeuN, MAP2, SMI312 and no primary antibody (-1Ab) or substrate BP (-BP). Samples of anti-NFASC, -1Ab, -BP, anti-NeuN, anti-MAP2 and anti-SMI312 were loaded as the ratio of 3: 3: 3: 1: 1: 1.

Figure S4

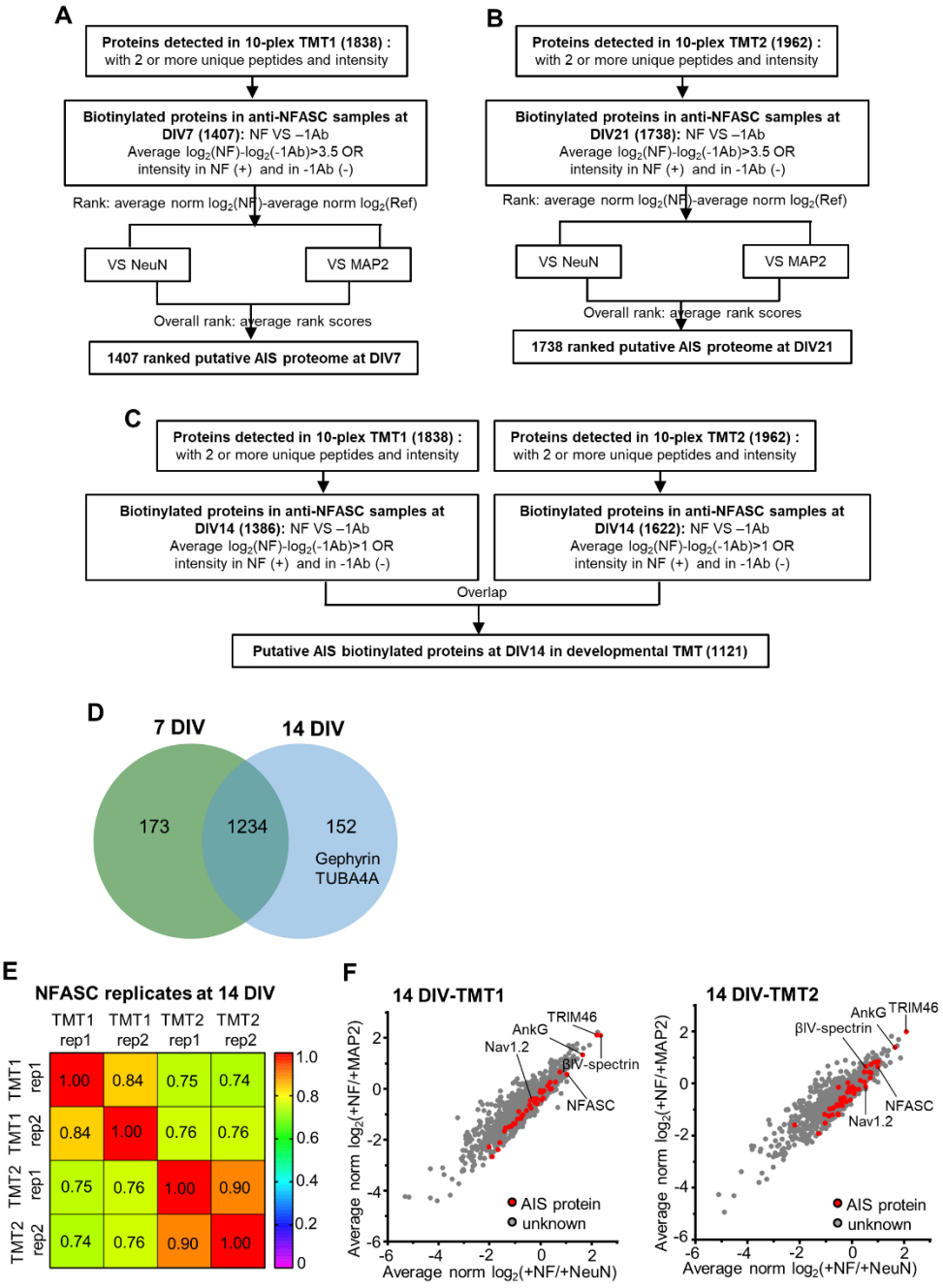
A
Proteins detected in 10-plex TMT1 (1838) :
with 2 or more unique peptides and intensity
Biotinylated proteins in anti-NFASC samples at DIV7 (1407): NF VS –1Ab
Average log2(NF)-log2(-1Ab)>3.5 OR
intensity in NF (+) and in -1Ab (-)
Rank: average norm log2(NF)-average norm log2(Ref)
VS NeuN
VS MAP2
Overall rank: average rank scores
1407 ranked putative AIS proteome at DIV7
B
Proteins detected in 10-plex TMT2 (1962) :
with 2 or more unique peptides and intensity
Biotinylated proteins in anti-NFASC samples at DIV21 (1738): NF VS –1Ab
Average log2(NF)-log2(-1Ab)>3.5 OR
intensity in NF (+) and in -1Ab (-)
Rank: average norm log2(NF)-average norm log2(Ref)
VS NeuN
VS MAP2
Overall rank: average rank scores
1738 ranked putative AIS proteome at DIV21
C
Proteins detected in 10-plex TMT1 (1838) :
with 2 or more unique peptides and intensity
Proteins detected in 10-plex TMT2 (1962) :
with 2 or more unique peptides and intensity
Biotinylated proteins in anti-NFASC samples at DIV14 (1386): NF VS –1Ab
Average log2(NF)-log2(-1Ab)>1 OR
intensity in NF (+) and in -1Ab (-)
Biotinylated proteins in anti-NFASC samples at DIV14 (1622): NF VS –1Ab
Average log2(NF)-log2(-1Ab)>1 OR
intensity in NF (+) and in -1Ab (-)
Overlap
Putative AIS biotinylated proteins at DIV14 in developmental TMT (1121)
D
7 DIV
14 DIV
173
1234
152
Gephyrin
TUBA4A
E
NFASC replicates at 14 DIV
TMT1 rep1
TMT1 rep2
TMT2 rep1
TMT2 rep2
1.00 0.84 0.75 0.74
0.84 1.00 0.76 0.76
0.75 0.76 1.00 0.90
0.74 0.76 0.90 1.00
1.0
0.8
0.6
0.4
0.2
0
F
14 DIV-TMT1
TRIM46
AnkG
Nav1.2
βIV-spectrin
NFASC
AIS protein
unknown
Average norm log2(+NF/+MAP2)
Average norm log2(+NF/+NeuN)
14 DIV-TMT2
AnkG
TRIM46
βIV-spectrin
NFASC
Nav1.2
AIS protein
unknown
Average norm log2(+NF/+MAP2)
Average norm log2(+NF/+NeuN)

Figure S4. Related to Figure 3. Analysis of AIS developmental proteome.

(A-C) Workflow for DIV7 (A), 21 (B) and 14 (C) biotinylated proteins analysis in anti-NFASC samples.

(D) Venn analysis of anti-NFASC targeted biotinylated proteins between DIV7 and 14 in 10-plex TMT1.

(E-F) Analysis of DIV14 anti-NFASC targeted biotinylated proteins from two parallel TMT experiments. (E) Correlation analysis of biological replicates showing high reproducibility in anti-NFASC targeted AIS proximity labeling proteome from two 10-plex TMT experiments. (F) Scatterplot showing the enrichment of anti-NFASC targeted biotinylated proteins against soma (x-axis) and somatodendrites (y-axis). Red dots indicate reported AIS components and gray dots are proteins having no AIS information.

Figure S5

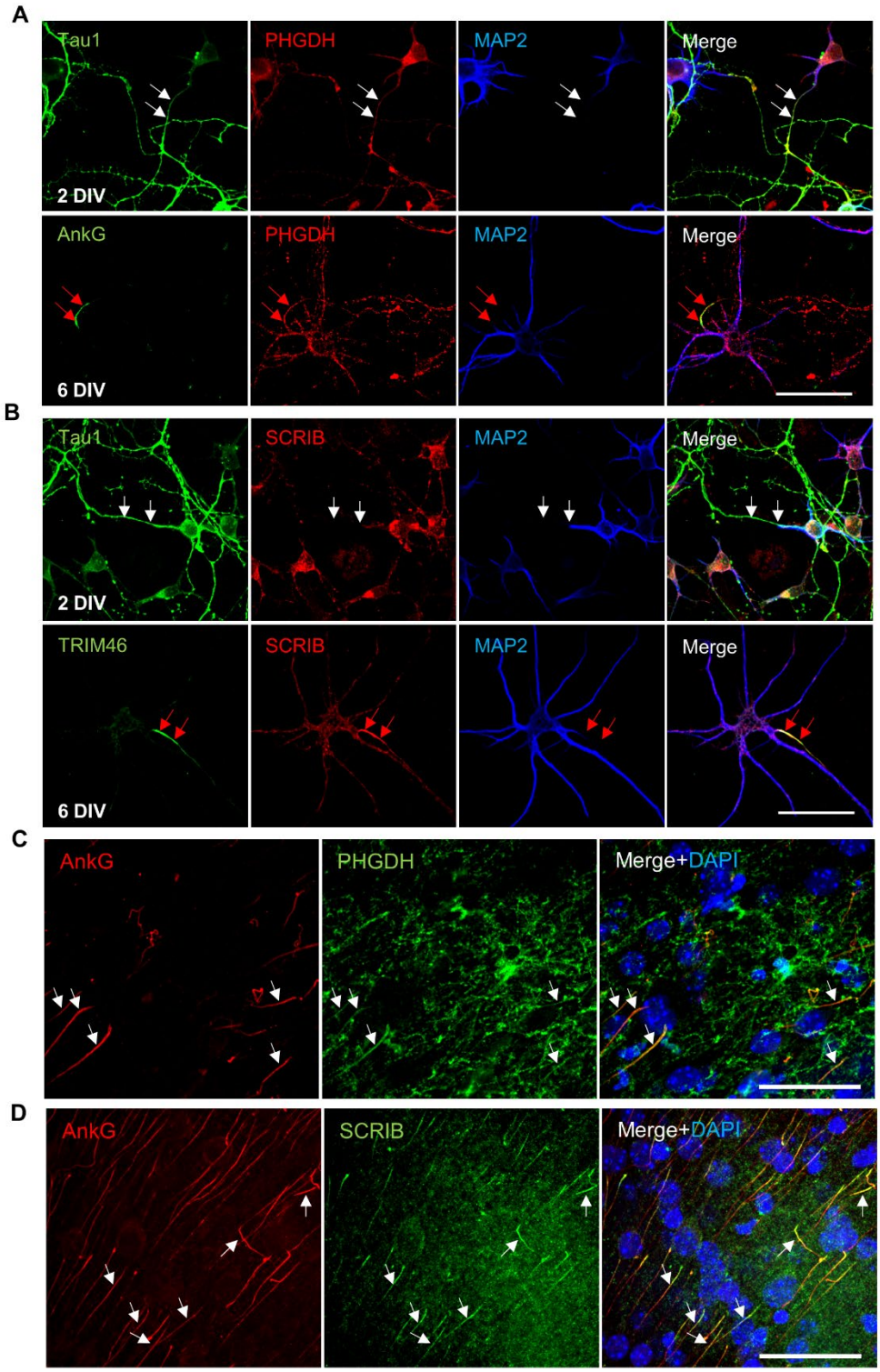
A
Tau1
PHGDH
MAP2
Merge
2 DIV
AnkG
PHGDH
MAP2
Merge
6 DIV
B
Tau1
SCRIB
MAP2
Merge
2 DIV
TRIM46
SCRIB
MAP2
Merge
6 DIV
C
AnkG
PHGDH
Merge+DAPI
D
AnkG
SCRIB
Merge+DAPI

Figure S5. Related to Figure 4. PHGDH and SCRIB expression in early developing neurons and brain slices.

(A) Representative images of DIV2 or 6 cortical neurons stained with PHGDH (red), MAP2 (blue, somatodendrites) and Tau1 (green, axon) or AnkG (green, AIS). White arrows indicate proximal axons and red arrows indicate axon initial segments. Bar= 50 μm.

(B) Representative images of DIV2 or 6 cortical neurons stained with SCRIB (red), MAP2 (blue, somatodendrites) and Tau1 (green, axon) or TRIM46 (green, AIS). White arrows indicate proximal axons and red arrows indicate axon initial segments. Bar= 50 μm.

(C-D) Coronal cortical sections from postnatal day 7 mice were stained with AnkG (red) and PHGDH (green, C) or SCRIB (green, D). Nuclei were stained with DAPI (blue). Arrows indicate the colocalization between AnkG signal and PHGDH or SCRIB staining. Bar= 50 μm.

Figure S6

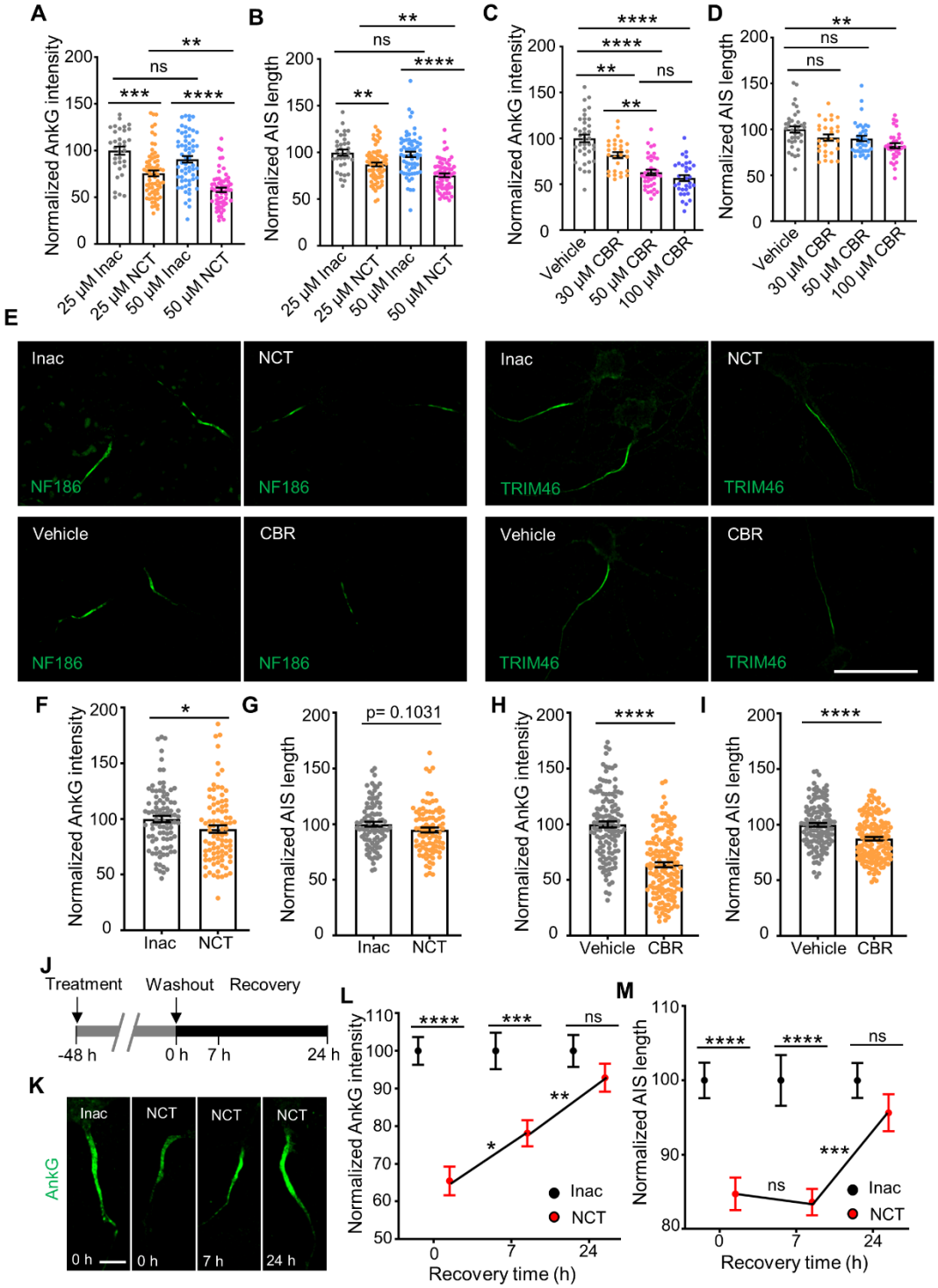
A
Normalized AnkG intensity
25 μM Inac
25 μM NCT
50 μM Inac
50 μM NCT
B
Normalized AIS length
C
Normalized AnkG intensity
Vehicle
30 μM CBR
50 μM CBR
100 μM CBR
D
Normalized AIS length
E
Inac
NCT
NF186
TRIM46
Vehicle
CBR
F
Normalized AnkG intensity
G
Normalized AIS length
p= 0.1031
H
Normalized AnkG intensity
I
Normalized AIS length
J
Treatment
Washout
Recovery
-48 h
0 h
7 h
24 h
K
AnkG
L
Normalized AnkG intensity
Recovery time (h)
M
Normalized AIS length
Recovery time (h)

Figure S6. Related to Figure 5. Inhibition of PHGDH activity decreases AIS components and AIS length.

(A-B) PHGDH inhibition by 25 and 50 μM NCT503 for 48 h reduces AnkG intensity in the AIS (A) and shortens AIS length (B). Data are normalized against 25 μM Inac samples. Two times independent experiments were performed. Graphs are presented as mean ± SEM. Statistical analysis was applied to AnkG intensity using Kruskal-Wallis test with Dunn's correction and AIS length using Tukey's multiple comparisons test. ****$p<0.0001$; ***$p<0.001$; **$p<0.01$; ns, not significant.

(C-D) PHGDH inhibition by CBR5884 for 48 h treatment reduces AnkG intensity (C) and AIS length (D). DIV19 cortical neurons were treated with 30, 50 and 100 μM PHGDH inhibitor CBR5884 for 48 h. Data are normalized against vehicle. Graphs are presented as mean ± SEM. Statistical analysis was applied to AnkG intensity using Tukey's multiple comparisons test and AIS length using Kruskal-Wallis test with Dunn's correction. ****$p<0.0001$; **$p<0.01$; ns, not significant.

(E) Representative images of cortical neurons showing NF186 and TRIM46 decrease after 48 h treatment with 50 μM PHGDH inhibitor NCT503 or CBR5884. Bar= 50 μm.

(F-G) 3 h treatment with 50 μM NCT503 leads to significant reduction of AnkG intensity (F) and slight shortening of AIS length (G). DIV11-15 neurons were treated with 50 μM NCT503 or Inac. Data are normalized against control. Two times independent experiments were performed. Graphs are presented as mean ± SEM. Mann-Whitney test, *$p<0.05$.

(H-I) 3 h treatment with 50 μM CBR5884 leads to significant reduction of AnkG intensity (H) and AIS length (I). DIV11-19 cortical neurons were treated with CBR5884 or vehicle DMSO. Three times independent experiments were performed. Graphs are presented as mean ± SEM. Mann-Whitney test, ****$p<0.0001$.

(J) Workflow for recovery experiments after PHGDH inhibition. Cortical neurons were first treated with 50 μM NCT503 or Inac for 48 h, followed by twice washout and then maintained in conditioned medium for 7 h and 24 h individually for recovery.

(K) Representative images of DIV14 neurons stained by AnkG antibody showing AIS structure recovery after 24 h maintenance in conditioned medium.

(L-M) Quantification of integrated AnkG intensity (L) in the AIS or AIS length (M) after different recovery periods (0, 7 and 24 h). Data are normalized against the corresponding control in each time point. Two times independent experiments were performed. Graphs are presented as mean ± SEM. Statistical analysis was applied to AnkG intensity using Mann-Whitney test and AIS length using Unpaired t-test. ****$p<0.0001$; ***$p<0.001$; **$p<0.01$; *$p<0.05$; ns, not significant.

KEY RESOURCES TABLE

Reagents, antibodies, and plasmids used in this study are summarized below:

REAGENT or RESOURCE	SOURCE	IDENTIFIER
Antibodies		
Mouse anti-Pan-Neurofascin	NeuroMab	Cat# 75-172, Clone A12/18
Mouse anti-AnkG	NeuroMab	Cat# 75-146, Clone N106/36
Chicken anti-AnkG	Synaptic Systems	Cat# 386006, Lot: 1-2
Chicken anti-TRIM46	Synaptic Systems	Cat# 377006, Lot: 1-1
Mouse anti-NeuN	Abcam	Cat# ab104224
Mouse anti-MAP2	Sigma-Aldrich	Cat# M1406, Clone AP-20
Chicken anti-MAP2	Abcam	Cat# ab5392, Lot: GR3297672-5
Chicken anti-MAP2	Encor	Cat# CPCA-MAP2
Mouse anti-Neurofilament (pan axonal, cocktail)	Biolegend	Cat# 837904, clone SMI312
Rabbit anti-PHGDH	Abclonal	Cat# A10461, Lot: 3508759001
Rabbit anti-PHGDH	Atlas antibodies	Cat#HPA021241 Lot: 000025827
Rabbit anti-SCRIB	Abclonal	Cat# A17450, Lot: 0098460101
Rabbit anti-βIV-spectrin	Gift of Dr. Matthew Rasband (BCM)	RRID: AB_2315634
Mouse anti-Tau1	Merk-Millipore	Cat# MAB3420, clone PC1C6
Mouse anti-V5	Invitrogen	Cat# R960CUS
Goat anti-Mouse IgG2a, Alexa Fluor 488	Invitrogen	Cat# A21131
Goat anti-mouse IgG (H+L), Alexa Flour 488	Invitrogen	Cat# A11029
Goat anti-mouse IgG (H+L), Alexa Flour 568	Invitrogen	Cat# A11031
Goat anti-rabbit IgG (H+L), Alexa Flour 488	Invitrogen	Cat# A11034

Goat anti-rabbit IgG (H+L), Alexa Flour 568	Invitrogen	Cat# A11036
Goat anti-chicken IgY (H+L), Alexa Flour 488	Invitrogen	Cat# A11039
Goat anti-chicken IgY (H+L), Alexa Flour 647	Invitrogen	Cat# A21449
Goat anti-mouse IgG, STAR-Red	Abberior	Cat# STRED-1001
Streptavidin-Alexa Fluor 568	Invitrogen	Cat# S11226
Streptavidin-Alexa Fluor 647	Invitrogen	Cat# S21374
Streptavidin-HRP conjugate	Invitrogen	Cat# 21124
Anti-mouse IgG, HRP-linked antibody	Cell signaling technology	Cat# 7076S
Anti-chicken IgY (H+L), HRP-linked antibody	Invitrogen	Cat# A16054
Anti-chicken IgY (H+L), HRP-linked antibody	Abcam	Cat# ab6877
Chemicals, Peptides, and Recombinant Proteins		
NCT503	GLPBIO	Cat# GC15943
PHGDH-inactive	GLPBIO	Cat# GC17293
CBR5884	GLPBIO	Cat# GC13336
Neurobasal Medium	Gibco	Cat# 21103-049
B-27 supplement	Gibco	Cat# 17504-044
GlutaMax-I	Gibco	Cat# 35050-061
Penicillin-Streptomycin	Gibco	Cat# 15140122
DMEM medium	Gibco	Cat# C11995500BT
Fetal bovine serum	Gibco	Cat# 100099044
2.5% trypsin	Invitrogen	Cat# 15090-046
Hank's buffered salt solution (HBSS)	Gibco	Cat# 14185-052
HEPES	Gibco	Cat# 15630-080
Cytosine β-D-arabinofuranoside hydrochloride (AraC)	Sigma	Cat# C6645
DNase	Sigma	Cat# DN25
Poly-D-lysine	Sigma	Cat# P7280
Laminin mouse protein	Gibco	Cat# 23017015
Lipofectamine 3000 Reagent	Invitrogen	Cat# L3000008
40% formaldehyde	Aladdin	Cat# F111934
Phosphate buffer saline (PBS)	Solarbio	Cat# P1020
Tween-20	Solarbio	Cat# T8220
Glycine	Solarbio	Cat# G8200
N-Ethyl-N-(3-dimethylaminopropyl) carbodiimide hydrochloride (EDCI)	Sigma-Aldrich	Cat# E7750

Dimethylformamide	Sigma-Aldrich	Cat# 189979
N-hydroxysuccinimide	Sigma-Aldrich	Cat# 130672
Ethanol	ThermoFisher	Cat# E7023
Dimethyl sulfoxide	Sigma-Aldrich	Cat# D8418
Tyramine	Sigma-Aldrich	Cat# T90344
4-(2-aminoethyl)aniline	Sigma-Aldrich	Cat# 123056
Dichloromethane	Sigma-Aldrich	Cat# 270997
2-Propanol	Sigma-Aldrich	Cat# 278475
4-Methoxyphenol	Sigma-Aldrich	Cat# M18655
4-Methoxyaniline	Sigma-Aldrich	Cat# A88255
Boron tribromide	Sigma-Aldrich	Cat# 230367
N-Boc-ethylenediamine	Sigma-Aldrich	Cat# 15369
4-Hydroxybenzoic acid	Sigma-Aldrich	Cat# 240141
1-Hydroxybenzotriazole hydrate (HOBt)	Sigma-Aldrich	Cat# 157260
Triethylamine	Sigma-Aldrich	Cat# T0886
Probe BP	This paper	N/A
Probe BP2	This paper	N/A
Probe BP3	This paper	N/A
Probe BP4	This paper	N/A
Probe BA1	This paper	N/A
Probe BA2	This laboratory	N/A
Hydrogen peroxide (H_2O_2)	Tongguang	Cat# 106057
Sodium ascorbate	Aladdin	Cat# S105024
Trolox	Sigma	Cat# 238813
DAPI	Invitrogen	Cat# D1306
Fluoromount-G	SouthernBiotech	Cat# 0100-01
Tris-base	Sigma	Cat# V900483
Sodium chloride (NaCl)	Tongguang	Cat# 112008
Sodium chloride (NaCl)	Sigma-Aldrich	Cat# S3014
Potassium chloride (KCl)	Sigma-Aldrich	Cat# P9541
Calcium chloride ($CaCl_2$)	Sigma-Aldrich	Cat# 21108
Magnesium chloride ($MgCl_2$)	Sigma-Aldrich	Cat# M2670
HEPES	Sigma-Aldrich	Cat# H3375
Sucrose	Sigma-Aldrich	Cat# V900116
Sodium hydroxide (NaOH)	Xilong Scientific Co., Ltd.	Cat# 10103101

Potassium hydroxide (KOH)	Xilong Scientific Co., Ltd.	Cat# 10202101
Cesium hydroxide (CSOH)	Sigma-Aldrich	Cat# 232041
Cesium chloride (CsCl)	Sigma-Aldrich	Cat# C4036
EGTA	Sigma-Aldrich	Cat# E3889
TEA-Cl	Sigma-Aldrich	Cat# 113042
Cadmium chloride ($CdCl_2$)	Aladdin	Cat# C118631
K-gluconate	Sigma-Aldrich	Cat# G4500
Mg-ATP	Shanghai yuanye Bio-Technology Co., Ltd	Cat# R21326
5'-GTP, 2Na	Shanghai yuanye Bio-Technology Co., Ltd	Cat# S18078
D-Glucose	Sigma-Aldrich	Cat# G7021
NBQX	Abcam	Cat# ab120046
D-APV	Abcam	Cat# ab120003
Gabazine	Abcam	Cat# ab120042
Biocytin	Sigma-Aldrich	Cat# B4261
Sodium deoxycholate	Sigma	Cat# 30970
Sodium dodecyl sulfate (SDS)	Solarbio	Cat# S8010
Protease inhibitors cocktail	Roche	Cat# 04693132001
PVDF membrane	Bio-Rad	Cat# 1620177
Bovine albumin	Sangon Biotech	Cat# A600332
Precision Plus Protein Dual Color Standards	Bio-Rad	Cat# 1610394
TBST	Biorigin	Cat# BN20543
Streptavidin agarose resin	ThermoFisher	Cat# 20353
D-biotin	Sigma	Cat# B4639
Clarity western ECL substrate	Bio-Rad	Cat# 1705060
Methanol	ThermoFisher	Cat# AAB-A456-4
Urea	Sigma	Cat# U1250
Dithiothreitol	Sigma	Cat# D9163
Iodoacetamide	Sigma	Cat# I6125
Triethylammonium bicarbonate buffer (TEAB)	Sigma	Cat# T7408
Sequencing-grade trypsin	Promega	Cat# V511A
Acetonitrile	Fisher	Cat# A998-4
Trifluoroacetic acid (TFA)	Macklin	Cat# T818782
Formic acid	Fluka	Cat# 94318

HCHO	Sigma	Cat# 252549
$^{13}CD_2O$	Sigma	Cat# 596388
Ammonia solution ($NH_3 \cdot H_2O$)	Aladdin	Cat# A112079
50% Hydroxylamine	ThermoFisher	Cat# 90115
Critical Commercial Assays		
EndoFree Mini Plasmid Kit II	Tiangen	Cat# DP118-02
BCA Protein Assay Kit	ThermoFisher	Cat# 23227
Quantitative Colorimetric Peptide Assay	ThermoFisher	Cat# 23275
Fast Silver Stain Kit	Beyotime	Cat# P0017S
High pH Reversed-Phase Peptide Fractionation Kit	ThermoFisher	Cat# 84868
TMT 10-plex Mass Tag Labeling Kits and Reagents	ThermoFisher	Cat# 90110, Lot: UL291038
Experimental models: Organisms/ Strains		
Rat: Sprague-Dawley rat pups (P0)	Peking University Health Science Center	N/A
Mouse: wild-type C57BL/6 (P7)	Beijing Vital River Laboratory Animal Technology Co., Ltd.	https://www.vitalriver.com/
Oligonucleotides		
Guide RNA (gRNA) targets for *Phgdh* knock-in: AGTGTCTCCGTCAGACACCT	This paper	N/A
Guide RNA (gRNA) targets for *Scrib* knock-in: GGGAAGCACCTGGCCCTAGG	This paper	N/A
Recombinant DNA		
PX551 (AAV-SpCas9)	Gift of Dr. Feng Zhang	Addgene #60957
pCAG_smFP V5	Gift of Dr. Loren Looger	Addgene #59758
pUCmini-iCAP-PHP.S	Gift of Dr. Viviana Gradinaru	Addgene #103002
pHelper	Agilent Technologies	Cat #240071
Knock-in sgRNA and donor for PHGDH	This paper	N/A
Knock-in sgRNA and donor for SCRIB	This paper	N/A
Software and Algorithms		
MaxQuant software (version 1.6.10.43)	Max Planck Institute of Biochemistry	https://www.maxquant.org/
Fiji-ImageJ	NIH	https://fiji.sc/

GraphPad Prism 8	GraphPad	https://www.graphpad.com/
MATLAB (R2019B, Simulink)	Mathworks	https://www.mathworks.com/products/matlab.html
LabVIEW (version 15.0)	National Instruments	https://www.ni.com/zh-cn/shop/labview.html
R studio (version 4.2.0)	The R Foundation	https://www.rstudio.com/
Huygens Essential (version 21.10)	Scientific Volume Imaging	https://svi.nl/Huygens-Essential

METHOD DETAILS

Probe synthesis

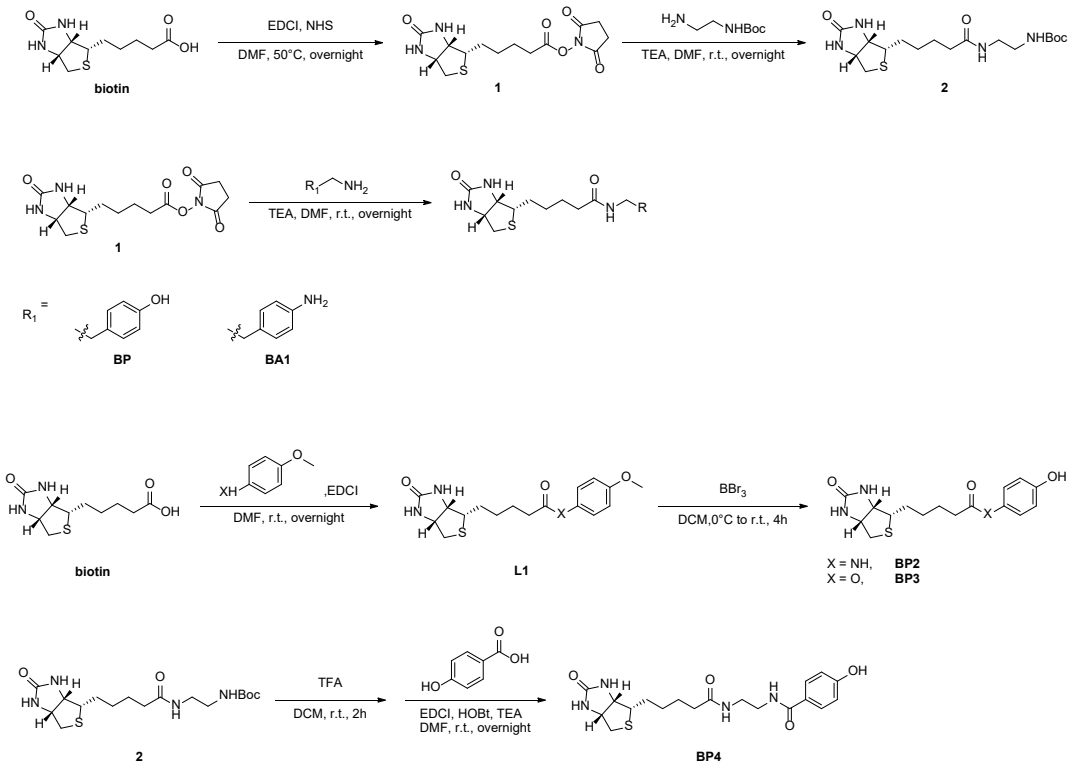

Synthesis of compound **1**

To a solution of D-biotin (1.76 g, 7.2 mmol) and EDCI (1.54 g, 8.0 mmol) in 50 ml DMF, N-hydroxysuccinimide (0.92 g, 8.0 mmol) was added at room temperature (RT). The reaction mixture was stirred at 50°C overnight. DMF was removed under vacuum to a residue of 5 ml. Add 100 ml cold ethanol into the residue during which time a white precipitate formed. Precipitate was filtered and washed with 15 ml ethanol twice, then dried in vacuum to afford compound **1**. The yield was 73%.

^{1}H-NMR (400 MHz, d_6-DMSO): 6.43 (1H, s), 6.37 (1H, s), 4.30 (1H, m), 4.15 (1H, m), 3.11 (2H, m), 2.84 (1H, dd), 2.81 (4H, s), 2.67 (2H, t), 2.60 (1H, d), 1.75-1.30 (6H, m).

Synthesis of compound **2**

Trimethylamine (1.60 g, 16 mmol) was added to a solution of mono-Boc protected ethylene diamine (1.66 g, 10 mmol) and compound **1** (1.76 g, 5.2 mmol) in 50 ml DMF. The reaction mixture was stirred at RT overnight and concentrated by rotary evaporation. The residue was dissolved in a solution of DCM and ^{i}PrOH (v/v = 4:1) and washed with 20 ml 1 M HCl followed by 20 ml water three times. The organic layers were combined and evaporated, and the residue was purified by column chromatography, affording compound **2**. The yield was 72%.

^{1}H-NMR (400 MHz, d_6-DMSO): 7.79 (1H, t), 6.79 (1H, t), 6.43 (1H, s), 6.36 (1H, s), 4.30 (1H, m), 4.13 (1H, m), 3.05 (3H, m), 2.96 (2H, m), 2.81 (1H, dd), 2.59 (1H, d), 2.04 (2H, t), 1.68-1.41 (4H, m), 1.37 (9H, s), 1.34- 1.19 (2H, m).

Synthesis of **BP** and **BA1**

To a solution of compound **1** (0.50 g, 1 e.q.) and corresponding primary amine (1.1 e.q.) in 50 ml DMF, trimethylamine (3 e.q.) was added to the mixture and stirred overnight at RT. The reaction solvent was evaporated and the residue was purified by C18 reverse phase column (Waters XBridge Prep C18 5 μm OBD 19x150 mm) on semi-preparative UPLC (Waters 2998 Photodiode Array Detector and 2545 Binary Gradient Module) with a gradient of 3% to 60% methanol in water over 25 min. The overall yields were 60-70%.

^{1}H-NMR for **BP** (400 MHz, d_6-DMSO): 9.13 (1H, s), 7.79 (1H, t), 6.97 (2H, d), 6.66 (2H, d), 6.42 (1H, s), 6.35 (1H, s), 4.31 (1H, m), 4.12 (1H, m), 3.18 (2H, dd), 3.08 (1H, m), 2.83 (1H, dd), 2.57 (3H, m), 2.03 (2H, t), 1.65-1.39 (4H, m), 1.35-1.19 (2H, m).

^{1}H-NMR for **BA1** (400 MHz, d_6-DMSO):7.78 (1H, t), 6.84 (2H, d), 6.49 (2H, d),6.43 (1H, s), 6.36 (1H, s), 4.85 (2H, s), 4.31 (1H, m), 4.12 (1H, m), 3.16 (2H, dd), 3.09 (2H, dd),2.84 (1H, dd), 2.56 (3H, m), 2.03 (2H, t), 1.38-1.66 (4H, m), 1.28 (2H, m).

Synthesis of **BP2** and **BP3**

To a solution of D-biotin (1.00 g, 4.0 mmol), EDCI (0.85 g, 4.5 mmol) in 30 ml DMF, corresponding phenol or aniline (0.56 g, 4.5 mmol) was added and the reaction mixture was stirred at RT overnight. The reaction mixture was evaporated, and the residue was purified by column chromatography, affording compound **L1**.

To the solution of **L1** in 20 ml DCM, BBr_3 (1.0 ml, 10 mmol) was added to the mixture dropwise at 0°C. After being stirred at 0°C for 4 h, the mixture was heated to RT and continued to react for 12 h. Then, 50 ml water was added to the mixture, and the residue was washed by 10 ml cold water for three times, and purified by semi-preparative column to get the purified product **BP2** or **BP3**. The whole yield was 25%.

^{1}H-NMR for **BP2** (400 MHz, d_6-DMSO): 9.60 (s, 1H), 9.13 (s, 1H), 7.35 (d, 2H), 6.67 (d, 2H), 6.45 (s, 1H), 6.37 (s, 1H), 4.31 (m, 1H), 4.14 (m, 1H), 3.14 (m, 1H), 2.84 (dd, 1H), 2.59 (d, 1H), 2.25 (t, 2H), 1.69-1.46 (m, 4H), 1.42-1.27 (m, 2H).

^{1}H-NMR for **BP3** (400 MHz, d_6-DMSO): 9.44 (s, 1H), 6.90 (m, 2H), 6.76-6.74 (m, 2H), 6.47 (s, 1H), 6.38 (s, 1H), 4.31 (m, 1H), 4.15 (m, 1H), 3.13 (m, 1H), 2.83 (dd, 1H), 2.58 (d, 1H), 2.53 (m, 2H), 1.71-1.47 (m, 4H), 1.45-1.34 (m, 2H).

Synthesis of **BP4**

Compound **2** (0.45 g, 1.2 mmol) was dissolved in 15 ml TFA/DCM (v/v= 1:1) and stirred at RT for 2 h. The solvent was removed under vacuum and the residue was dissolved in 20 ml DMF. To this solution was added 4-Hydroxybenzoic acid (0.15 g, 1.2 mmol), EDCI (0.45 g, 2.4 mmol), HOBt (0.35 g, 2.4 mmol), and TEA (0.36 g, 3.5 mmol). The reaction mixture was stirred at RT overnight. Then, the reaction mixture was evaporated, and the residue was purified by C18 reverse phase column (Waters XBridge Prep C18 5 μm OBD 19x150 mm) on semi-preparative UPLC (Waters 2998 Photodiode Array Detector and 2545 Binary Gradient Module) with a gradient of 3% to 80% methanol in water over 30 min. The overall yields were 50%.

^{1}H-NMR (400 MHz, d_6-DMSO): 8.21 (t, 1H), 7.90 (t, 1H), 7.69 (d, 2H), 6.85 (d, 2H), 6.39 (d, 2H), 4.29 (dd, 1H), 4.14 (m, 1H), 3.03 (ddd, 1H), 2.80 (dd, 1H), 2.57 (d, 1H), 2.06 (t, 2H), 1.67-1.19 (m, 6H).

Primary neuron culture

Briefly, cortexes or hippocampi of neonatal P0 Sprague-Dawley pups were dissected and incubated in a digestion solution (0.25% trypsin and 0.4 mg/ml DNase in Ca^{2+}/Mg^{2+} free HBSS) at 37°C for 15 min. Followed by the dissociation using fire-polished Pasteur pipettes, neurons were placed on 100 μg/ml poly-D-lysine (Sigma) coated 10-cm dishes at a density of 100,000 cells/cm^2 or on coverslips coated by 20 μg/ml poly-D-lysine and 10 μg/ml laminin mouse protein (Gibco) at a density of 40,000 cells/cm^2 in plating medium (high glucose DMEM medium containing L-glutamine and 10% fetal bovine serum). After 3 h, the medium was changed into neuronal culture medium (Neurobasal, B27 supplement, Glutamax-I and penicillin-streptomycin) to maintain neuronal long-term growth. 2 μM cytosine β-D-arabinofuranoside hydrochloride (AraC) was added after 6 days to slow down glia cells proliferation. One third of culture medium was replaced with fresh neuronal culture medium every seven days.

Low density cortical neuron culture was prepared as previously described [1,2]. In the co-culture model, neurons were grown on coverslips suspended above an astrocyte feeder layer by paraffin points. Neurons were plated on coverslips at a density of 10,000 cells/cm^2 for 3 h in plating medium. Then coverslips were inverted and transferred to culture dishes with 60~70% astrocytes monolayer in neuronal culture medium. 5 μM AraC was added after 1~2 days plating to curb glia cells proliferation. One third of culture medium was replaced with fresh neuronal culture medium every seven days.

Optimization of anti-NFASC antibody targeted AIS proximity labeling

Neurons were fixed with 4% formaldehyde for 15 min at RT. The free aldehyde group was quenched by 0.25 M Glycine for 10 min. After washing four times with PBS, endogenous peroxidase of cells was deactivated in 1.5% H_2O_2 as long as 1.5 h. Washed samples were blocked by 5% fetal bovine serum dissolved in PBS containing 0.1% Tween-20 for 1 h at RT. Then neurons were stained with 1, 2 or 5 μg/ml mouse anti-Pan-Neurofascin (anti-NFASC, NeuroMab, Cat# 75-172, stock 1 mg/ml) dissolved in antibody dilution solution (1% FBS with 0.1% Tween-20 in PBS) for 1 h at RT. Followed by washes in washing solutions (0.1% Tween-20 in PBS), samples were labelled with 0.1, 0.2, 0.5 or 1 μg/ml HRP conjugated anti-mouse IgG (Cell signaling technology, Cat# 7076S, stock 1 mg/ml) for 1 h. Samples were washed for another four times with washing solution and incubated with 6 different probes (see supplementary Figure S1E) individually at a concentration of 500 μM for 10 min. The proximity labeling was triggered with the addition of H_2O_2 (1, 100, 500 or 1000 μM). After 1, 5 or 10-min reaction, the proximity labeling was stopped by adding quenching solutions (50 mM sodium ascorbate and 5 mM Trolox dissolved in PBS). Endogenous bait protein NFASC and biotinylated proteins were detected by immunocytochemistry to compare proximity labeling specificity and efficiency through imaging.

Antibody targeted proximity labeling

The above optimized parameters were applied to anti-NFASC, anti-NeuN, anti-MAP2 and anti-SMI312 targeted AIS, soma, somatodendrites and axon proximity labeling. The blocked samples were stained with primary antibodies dissolved in antibody dilution solution (1% FBS with 0.1%Tween-20 in PBS) for 1 h at RT. After washing, samples were labelled with HRP conjugated second antibodies for 1 h and then incubated with 500 μM biotin-phenol (BP) for 10 min. The proximity labeling was triggered with the addition of 100 μM H_2O_2. After 1 min reaction, free radicals were quickly quenched twice by quenching

solutions (50 mM sodium ascorbate and 5 mM Trolox dissolved in PBS). Samples were finally washed with PBS.

In the case of anti-AnkG and anti-TRIM46 targeted proximity labeling, parameters including antibody dilutions and H_2O_2 concentration were also individually tested. Antibodies used for proximity labeling were listed as follows. Primary antibodies: mouse anti-Pan-Neurofascin (anti-NFASC, NeuroMab, Cat# 75-172), mouse anti-AnkG (NeuroMab, Cat# 75-146), mouse anti-NeuN (Abcam, Cat# ab104224), mouse anti-MAP2 (Sigma-Aldrich, Cat# M1406), mouse anti-Neurofilament (anti-SMI312, Biolegend, Cat# 837904), chicken anti-AnkG (Synaptic Systems, Cat# 386006) and chicken anti-TRIM46 (Synaptic Systems, Cat# 377006). HRP conjugated second antibodies: anti-mouse IgG (Cell signaling technology, Cat# 7076S) or anti-chicken IgY (Invitrogen, Cat# A16054; Abcam, Cat# ab6877).

Protein lysis of cortical neurons after proximity labeling

Dimethyl experiments include three pairs: anti-NFASC vs. no primary antibody; anti-NFASC vs. anti-NeuN; and anti-NFASC vs. anti-MAP2. Three times independent replicates were performed in each pair. The 10-plex TMT DIV14 MS experiment include: three biological replicates for anti-NFASC targeted proximity labeling; no primary antibody or BP probe negative controls; reference samples of anti-NeuN, anti-MAP2 (duplicates), and anti-SMI312 (duplicates). Due to differences in the bait abundance, references samples of anti-NeuN, anti-MAP2 and anti-SMI312 yielded higher amounts of labeled proteins than the anti-NFASC sample. To balance peptide loading to LC-MS/MS analysis, we used only a fraction of the reference samples for biotinylated proteins enrichment. Anti-NF186, no primary antibody and no substrate BP shared the same protein quantity for enrichment. 1/4~1/2 protein quantity was used for anti-NeuN, anti-MAP2 and anti-SMI312 enrichment (see figure legends).

In AIS developmental TMT experiments, two parallel 10-plex TMT experiments were performed and DIV14 samples were used as a reference for DIV7 and DIV21 samples. Proximity labelled samples at DIV14 were equally divided and used for TMT1 and TMT2 pipeline. Five conditions were designed for each stage: anti-NFASC targeted AIS proximity labeling (duplicates); no primary antibody (-1Ab); anti-NeuN targeted soma proximity labeling and anti-MAP2 targeted somatodendrites proximity labeling. An amount of 1.5 mg proteins in samples of anti-NFASC and no primary antibody (DIV7, 14 and 21) were used for enrichment, while 1/2 and 1/4 protein quantity were used for anti-NeuN and anti-MAP2 enrichment individually.

Proximity labeling samples were lysed with lysis solution (50 mM Tris-HCl pH 7.6, 150 mM NaCl, 1% SDS, 0.5% sodium deoxycholate, 1% Triton X-100 and protease inhibitors cocktail) on ice for 10 min. 500 µl lysis solution was added for each 10-cm dish. In the condition of anti-NFASC, no primary antibody and no substrate BP, three 10-cm dishes in one replicate were needed for protein lysis. While for anti-NeuN, anti-MAP2 and anti-SMI312 conditions, one or two 10-cm dishes were needed. Protein lysis were de-crosslinked at 99ºC for 1 h. Lysed solution was sonicated on ice and then centrifuged at 12,000 rpm for 10 min at 4ºC to collect supernatant. Proteins were precipitated in cold methanol at -80ºC freezer.

Enrichment of biotinylated proteins and on-bead digestion

Precipitated proteins were washed twice using cold methanol. Purified proteins were dissolved completely in 0.5% SDS (w/v). Protein concentration was measured through BCA Protein Assay Kit to adjust protein quantity for enrichment. 1% of pre-enrichment proteins were kept to test biotinylated signal via Western blotting or silver staining to assess proximity labeling efficiency. Left proteins were incubated with 200 µl streptavidin beads for 3 h with gentle rotation at RT. 5% of post-enrichment proteins were kept to test the enrichment efficiency via Western blotting or silver staining. Then the protein-beads

mixture was sequentially washed twice by 2% SDS (w/v), 8 M urea and 2 M sodium chloride. The mixture was reduced by 10 mM dithiothreitol and then with 20 mM iodoacetamide for alkylation. After four times washing with 100 mM TEAB, proteins on beads were digested with the addition of 2 μg trypsin (Promega, Cat# V511A) for 18 h at 37°C.

Western blotting and silver staining

Protein samples were heated at 99°C for 10 min with the addition of protein loading buffer. In the case of post-enrichment proteins, 2 mM biotin was added to elute biotinylated proteins. Proteins were loaded for electrophoresis in 5% SDS-PAGE stacking gel and 10% SDS-PAGE separating gel. The electroporated gel could be directly used for silver staining with the instructions of Fast Silver Stain Kit (Beyotime, Cat# P0017S) or transferred to PVDF membrane. The blots were blocked with 5% BSA in the TBST solution at RT for 1 h and then immersed with streptavidin-HRP (Invitrogen, Cat# 21124, 0.25 μg/mL) for biotinylation assay. After triple washing, the blots were developed by Clarity western ECL substrate (Bio-Rad, Cat# 1705060) and imaged in ChemiDoc MP Imaging System (Bio-Rad).

Dimethyl labeling

Enriched proteins were digested with trypsin and the resulting peptides were treated with isotope-encoded formaldehyde (heavy $D^{13}CDO$ for anti-NFASC samples and light HCHO for negative control/reference samples) and $NaBH_3CN$ for their $–NH_2$ groups methylation, resulting in a mass shift from 34.0631 Da to 28.0313 Da. For pairs of anti-NFASC and no primary antibody, peptides were combined directly and desalted by C18 tips (ThermoFisher, Cat#87784). For pairs of anti-NFASC/ anti-NeuN or anti-NFASC/ anti-MAP2, peptides were desalted first separately and then equal amounts of peptides were combined. Peptides concentration was measured by Quantitative Colorimetric Peptide

Assay Kit (ThermoFisher, Cat# 23275). Combined peptides were dried in a vacuum concentrator and ready for liquid chromatography-tandem mass spectrometry (LC-MS/MS).

10-plex TMT labeling and peptides fractionation

Digested peptides were desalted by C18 tips (ThermoFisher, Cat#87784). In the case of 14 DIV independent TMT experiments, desalted total peptides of anti-NF186, no primary antibody and no substrate BP were directly used for TMT labeling. Taking anti-NF186 peptides amount as reference, the same quantity of peptides from anti-NeuN, anti-MAP2 and anti-SMI312 conditions were prepared in advance. Peptide concentration was measured by Quantitative Colorimetric Peptide Assay Kit (ThermoFisher, Cat# 23275). In the case of AIS developmental TMT experiments, sample amount was controlled when performing enrichment. Therefore, these peptides were directly applied to TMT labeling.

TMT labeling was performed as instructed by TMT 10-plex Mass Tag Labeling Kits and Reagents (ThermoFisher, Cat# 90110). Briefly, TMT reagents were maintained at RT and reconstituted with 41 μl anhydrous acetonitrile for 0.8 mg vial of each tag. Peptides were reconstituted in 10 μl 100 mM TEAB and dissolved completely. Add 12.5 μl TMT solution into dissolved peptides and label for 2 h in the dark. The labeling in each condition was described in Figure 2B and 3A. The reaction was quenched by adding 8 μl 5% hydroxylamine and which was incubated for 15 min. Peptides from ten conditions were mixed and dried in a vacuum concentrator. Mixed peptides were re-dissolved in 300 μl 0.1% trifluoroacetic acid and fractionated according to the instructions of Pierce High pH Reversed-Phase Peptide Fractionation Kit (ThermoFisher, Cat# 84868). Samples were eluted by gradient acetonitrile of 10.0%, 12.5%, 15.0%, 17.5%, 20.0%, 22.5%, 25.0%, 50.0% solution in 0.1% triethylamine and defined as fraction 1-8 respectively. Fractions were combined as pairs of ‘1+5’, ‘2+6’, ‘3+7’ and ‘4+8’ and dried again in vacuum concentrators. Peptides were ready for LC-MS/MS.

Liquid chromatography and mass spectrometry

Peptides were reconstituted in 0.1% formic acid and separated in a loading column (100 μm × 2 cm) and a C18 separating capillary column (75 μm × 15 cm) packed in-house with Luna 3 μm C18(2) bulk packing material (Phenomenex, USA). A 2-h liquid chromatography (LC) was applied to peptides separation. The LC gradient was held at 2% for the first 8 minutes of the analysis, followed by an increase from 2% to 10% B from 8 to 9 minutes, an increase from 10% to 44% B from 9 to 123 minutes, and an increase from 44% to 99% B from 123 to 128 minutes (A: 0.1% formic acid in water and B: 80% acetonitrile with 0.1% formic acid).

Samples were analyzed by Orbitrap Fusion LUMOS Tribrid Mass Spectrometer. The precursors were ionized using an EASY-Spray ionization source (Thermo Fisher Scientific). Survey scans of peptide precursors were collected in the Orbitrap from 350-1600 Th with an advance gain control (AGC) target of 400,000, a maximum injection time of 50 ms, RF lens at 30%, and a resolution of 60,000 at 200 m/z. In the case of HCD scans, an automated scan range determination was enabled. An isolation window of 1.6 Th was used to select precursor ions with the quadrupole. Product ions were collected in the Orbitrap with the first mass of 110 Th, an AGC target of 50,000, a maximum injection time of 30 ms, HCD collision energy at 30%, and a resolution of 15,000. Monoisotopic precursor selection was enabled for peptide isotopic distributions, precursors of z = 2-7 were selected for data-dependent MS/MS scans for 3 s of cycle time, and dynamic exclusion was set to 15 s with a ±10 ppm window set around the precursor mono-isotope.

Mass spectrometry data analysis

Raw data files were loaded in MaxQuant software (version 1.6.10.43) and searched against Rattus norvegicus proteomes from uniport database (Taxonomy, 10116, downloaded on Nov 15th, 2020). Trypsin was selected as the digestion mode. In the case of searching dimethyl proteomics, the composition of Hx(6)C(2)H(-2) was replaced by

Hx(4)Cx(2) in heavy labels of DimethLys6 and DimethNter6. Cysteine acetylation (carbamidomethyl) was a fixed modification. Methionine oxidation and protein N-terminal acetylation were variable modifications. Re-quantify button in Misc. module and match between runs in Identification module were activated. In the case of 10-plex TMT proteomics, reporter ion MS2 was selected and 10-plex TMT was activated. Correction factors were added to the tags based on the reagent instructions (ThermoFisher, Cat# 90110, Lot: UL291038). In both cases, the false discovery rate was set to 0.01.

Proteome data analysis

Anti-NFASC targeted AIS proximity labeling was the positive group. Samples of no primary antibody or no substrate BP were negative controls for cutoff analysis, while anti-NeuN, anti-MAP2 or anti-SMI312 targeted soma, somatodendrites or axon proximity labeling were reference controls for ranking AIS candidates. Top ranked proteins would have more possibility to be expressed or enriched in the AIS.

In the case of dimethyl experiments, contaminants and proteins identified as reversed hits were removed. Proteins containing at least 2 unique peptides and quantified in at least two out of three independent replicates were retained for further analysis (anti-NFASC vs. anti-NeuN: 965; anti-NFASC vs. anti-MAP2: 802). Additionally, an H/L ratio > 1.5 was set as the cutoff for each replicate in the experiment of anti-NFASC versus no primary antibody, which resulted in the identification of 704 proteins. Proteins in three pairs were intersected and a total of 568 proteins were obtained. We normalized the H/L ratio against the medium in each column using the formula of '$\log_2$(H/L)-medium $\log_2$(H/L)' in +NFASC/+NeuN and +NFASC/+MAP2 replicates. Averaged normalized data was obtained from three replicates and used for distribution analysis.

In the case of DIV14 TMT experiments, contaminants and proteins identified as reversed hits were removed. Proteins with at least two unique peptides were kept. Ratios were calculated by division using their MS intensity. Parallel analysis was analyzed using

Pearson correlation. The average ratio of replicates was used for the following analysis. The cutoff ratio was set at 2 for +NFASC/-BP and +NFASC/-1Ab sequential analysis. A total of 1403 proteins were retained for further analysis. Ratios of +NFASC/+NeuN, +NFASC/+MAP2 and +NFASC/+SMI312 were normalized against the medium ratio in their corresponding column. Proteins were ranked based on average normalized log_2(+NFASC/+References, fold change) in a descending order. The final overall rank was based on the average rank scores against soma, somatodendrites and axon. Proteins in the top 200 against each reference were overlapped and a total of 71 proteins were obtained. Gene Oncology analysis of these 71 proteins was performed PANTHER overrepresentation test. A total of 2755 neuronal proteins in this TMT were used as a reference. Among them, 2744 proteins were valid data in Gene Oncology database. Top cellular compartment and molecular function terms were presented.

In the case of AIS developmental TMT experiments, two parallel 10-plex TMT labeling were employed to analyze AIS developing (DIV7), mature (DIV14) and completely mature (DIV21) proteome changes. Contaminants and proteins identified as reversed hits were removed. Proteins with at least two unique peptides were kept. Ratios were calculated by division using their MS intensity. Parallel analysis was analyzed using Pearson correlation. The average ratio of replicates was used for further analysis. Proteins were filtered with the standard of 'average log_2(+NFASC)-log_2(-NFASC)>3.5' for DIV7 and 21, while for DIV14 the standard was set as 'average log_2(+NFASC)-log_2(-NFASC)>1'. This setting was based on the endogenous biotinylated proteins distribution. Proteins with intensity in +NFASC condition, not in -NFASC condition were also retained. Ratios of +NFASC/+NeuN and +NFASC/+MAP2 were normalized against the medium ratio in their corresponding column in each time point. Proteins were ranked based on average normalized log_2(+NFASC/+References, fold change) in a descending order. The final overall rank was based on the average rank scores against soma and somatodendrites.

For analysis of AIS protein dynamics along neuronal development, biotinylated proteins at DIV7, 14 and 21 together with prior DIV14 biotinylated proteins were overlapped and revealed 549 common proteins in three stages. These proteins in the condition of anti-NFASC at DIV7, 14 and 21 were normalized based on endogenous biotinylated protein PCCA [3]. Among 549 proteins, 534 proteins were presented more than 20% changes of average MS intensity in at least one pair of time points. Heatmap was performed using cutree script in R package of pheatmap. AIS molecules identified in three stages were performed Z-scored normalized abundance analysis. Significant analysis and fold changes were analyzed regarding these AIS proteins according to a guide of statistics for proteomics data analysis [4].

Immunocytochemistry and immunohistochemistry

For immunocytochemistry, neurons were fixed in 4% formaldehyde for 15 min at RT and washed three times in PBS. Samples were blocked by 5% fetal bovine serum dissolved in PBS containing 0.1% Tween-20 for 1 h at RT. Then neurons were sequentially stained with primary antibodies and fluorescent second antibodies for 1 h at RT. Nuclei were stained with DAPI (Invitrogen, Cat# D1306). Primary antibodies used in this study were as follows: mouse anti-Pan-Neurofascin (NeuroMab, Cat# 75-172, 1:1000), mouse anti-AnkG (NeuroMab, Cat# 75-146, 1:1000), mouse anti-NeuN (Abcam, Cat# ab104224, 1:1000), mouse anti-MAP2 (Sigma-Aldrich, Cat# M1406, 1:1000), mouse anti-Neurofilament (Biolegend, Cat# 837904, 1:1000), chicken anti-AnkG (Synaptic Systems, Cat# 386006, 1:500), chicken anti-TRIM46 (Synaptic Systems, Cat# 377006, 1:500), chicken anti-MAP2 (Abcam, Cat# ab5392, 1:10000), rabbit anti-PHGDH (Abclonal, Cat# A10461, 1:50), rabbit anti-PHGDH (Atlas antibodies, Cat# HPA021241, 1:500), rabbit anti-SCRIB (Abclonal, Cat# A17450, 1:50), rabbit anti-βIV-spectrin (laboratory of Dr. Matthew Rasband in BCM, 1:1000), mouse anti-Tau1 (Merk-Millipore, Cat# MAB3420, 1:1000) and mouse anti-V5 (Invitrogen, Cat# R960CUS, 1:500). Fluorescent second antibodies used

for immunocytochemistry were as follows with 1:1000 dilutions: goat anti-mouse IgG2a, Alexa Fluor 488 (Invitrogen, Cat# A21131), goat anti-mouse IgG (H+L), Alexa Flour 488 (Invitrogen, Cat# A11029), goat anti-mouse IgG (H+L), Alexa Flour 568 (Invitrogen, Cat# A11031), goat anti-rabbit IgG (H+L), Alexa Flour 488 (Invitrogen, Cat# A11034), goat anti-rabbit IgG (H+L), Alexa Flour 568 (Invitrogen, Cat# A11036), goat anti-chicken IgY (H+L), Alexa Flour 488 (Invitrogen, Cat# A11039) and goat anti-chicken IgY (H+L), Alexa Flour 647 (Invitrogen, Cat# A21449). In the case of proximity labeling samples, biotinylated protein signal was detected by incubation with streptavidin conjugated with Alexa Fluor 568 (Invitrogen, Cat# S11226) or Alexa Fluor 647 (Invitrogen, Cat# S21374).

For immunohistochemistry, brains from postnatal day 7 (P7) C57BL/6 mice were quickly removed and 300 µm coronal slices were cut with a vibratome at 4°C in a solution (234 mM sucrose, 11 mM glucose, 26 mM $NaHCO_3$, 2.5 mM KCl, 1.25 mM NaH_2PO_4, 10 mM $MgSO_4$, and 0.5 mM $CaCl_2$), which was equilibrated with 95% O_2-5% CO_2. Cortical sections were fixed with 4% formaldehyde for 1 h at RT and washed three times in PBS. Slices were blocked for 2 h at RT in 10% fetal bovine serum dissolved in PBS containing 0.1% TritonX-100 and then incubated with mouse anti-AnkG (NeuroMab, Cat# 75-146, 1:500), rabbit anti-PHGDH (Abclonal, Cat# A10461, 1:50) or rabbit anti-SCRIB (Abclonal, Cat# A17450, 1:50) at 4°C overnight. After washing, slices were incubated in goat anti-mouse IgG (H+L), Alexa Flour 568 (Invitrogen, Cat# A11031, 1:500) and goat anti-rabbit IgG (H+L), Alexa Flour 488 (Invitrogen, Cat# A11034, 1:500). Sections were counterstained with DAPI and mounted to glass slides with Fluoromount-G (SouthernBiotech, Cat# 0100-01).

Images were acquired on an inverted fluorescence microscope (Nikon-TiE, Japan) equipped with a 40x1.3 NA oil immersion objective lens, confocal laser lines (OBIS 405, 488, 532, 561 and 637 nm, Coherent, USA), spinning disk confocal unit (Yokogawa CSU-X1, Japan) and scientific CMOS cameras (Hamamatsu ORCA-Flash 4.0 v2). The microscope, camera and lasers were controlled with a customer-built software written in

LabVIEW (National Instruments). Sections were imaged in the focal position or in z-stacks with a 0.5 µm step size at a resolution of 1500x1000 pixels. Z-projection was obtained in Fiji-ImageJ software. Figures were adjusted and prepared in Fiji-ImageJ and Adobe Photoshop CC2018.

Detergent extraction

Neurons were rinsed in PBS and incubated in the extraction buffer (pH 7.0, 30 mM PIPES, 1 mM MgCl2, 5 mM EDTA, 0.5% Triton X-100) for 3 minutes at 37°C as previously described [5]. Following detergent extraction, neurons were quickly rinsed in PBS and fixed in 4% formaldehyde for 15 min at RT. Washed samples were ready for immunocytochemistry.

V5 tag knock-in and imaging by microscopy

V5 tag knock-in sgRNA and donor constructs were generated following strategies similar to those described previously [6,7]. Adeno-associated virus (AAV) cell-lysates were produced using the AAVpro Purification Kit (All Serotypes) (Takara) with slight modifications. Briefly, HEK293T cells were transfected with AAV plasmid, helper plasmid, and serotype PHP.S plasmid with PEI Max (Polysciences, 24765). Cells were then incubated for 3 days, and then the HEK293T cells were collected. The cells were lysed using the AAV Extraction Solution A plus and B, and this crude AAV solution was used for neuronal transduction. An aliquot of 20 µl of the AAVs (10 µl of Cas9 and 10 µl of Knock-in sgRNA and donor in a well of a 12-well plate) was added to cultures at 0 DIV. The medium was replaced after 2 days of infection. Neurons were fixed at the indicated time points and used for immunocytochemistry.

Imaging was performed using a Zeiss AxioImager Z2 fitted with apotome for structured illumination. Images were captured using the Zeiss ZEN software. Stimulated

Emission Depletion (STED) microscopy was performed for super-resolution imaging using a STEDyCON (Abberior) system fitted to a Nikon Eclipse Ti2 microscope.

Pharmacology experiments

PHGDH inhibitor NCT503 (GLPBIO, Cat# GC15943) and its control non-active analogue PHGDH-inactive (GLPBIO, Cat# GC17293) were dissolved in DMSO and stored with a concentration of 10 mM. Inhibitor CBR5884 (GLPBIO, Cat# GC13336) was dissolved in DMSO with a concentration of 50 mM and the solvent DMSO was its control. Mature neurons (11-19 DIV) were treated with 50 μM PHGDH inhibitors for 3 h or 48 h. In the case of pharmacological treatments without astrocytes, mature neurons grown on the coverslips suspended above astrocytes feeder layer were transferred to new P35 dishes and treated with drugs for 3 h or 48 h in glia cells conditioned medium. Owing to 5 μM AraC was added after plating 1 day in this co-culture model, fewer astrocytes were on the coverslips.

Patch-clamp recordings

In all electrophysiology experiments, the borosilicate glass electrodes (Sutter Instrument) were pulled to a resistance of 2.5–5 MΩ via a P-97 micropipette puller (Sutter Instrument). The whole-cell recordings on cultured cortical neurons were established via an inverted microscope (Eclipse Ti, Nikon), an sCMOS camera (ORCA-Flash4.0 V2, Hamamatsu), an amplifier (Axopatch 200B, Axon Instruments). Data digitalization and devices synchronization were performed on two data acquisition (DAQ) boards (PCI-6733 and PCIe-6353, National Instrument) and controlled via software written in LabVIEW (National Instruments) and MATLAB (R2019B, Simulink). The input/output signals for the patch-clamp experiments were all digitized at 21159 Hz, and the input data were filtered with an internal 5-kHz Bessel filter in the amplifier and a Hum Bug 50/60 Hz noise

eliminator (Quest Scientific). All whole-cell recordings were performed at RT, and the cell membrane was ruptured at a holding voltage of -70 mV.

The whole-cell current clamp experiments were performed in the high-glucose Tyrode's (extracellular) solution containing 125 mM NaCl, 2.5 mM KCl, 1 mM $MgCl_2$, 3 mM $CaCl_2$, 1 mM EGTA, 30 mM glucose, and 10 mM HEPES (all from Sigma-Aldrich). The pH was adjusted to 7.3 with 5 M NaOH (Xilong Scientific Co., Ltd.), and the osmotic pressure was adjusted to 305–315 mOsm/kg with 1 M sucrose (Sigma-Aldrich), respectively. The patch pipette was filled with an internal solution consisting of 125 mM potassium gluconate, 8 mM NaCl, 0.6 mM $MgCl_2$, 0.1 mM $CaCl_2$, 1 mM EGTA, 10 mM HEPES (Sigma-Aldrich), 4 mM Mg-ATP, and 0.4 mM Na_2-GTP (Shanghai Yuanye Bio-technology), and its pH and osmotic pressure were adjusted to 7.3 with 5 M KOH (Xilong Scientific Co., Ltd.) and 290–300 mOsm/kg with 1 M sucrose. 0.5% w/v biocytin (Sigma-Aldrich) was added to the internal solution for visualizing the clamped cells. Before the test, 10 μM NBQX (AMPAR inhibitor, Abcam), 25 μM D-APV (NMDAR inhibitor, Abcam), and 20 μM Gabazine ($GABA_AR$ inhibitor, Abcam) were added into the extracellular buffer for intrinsic excitability evaluation. The cells were held at -70 mV to calculate the series resistance of the recording, the neurons' membrane resistance, and membrane capacitance from a 10-mV depolarization step (9 Hz, 20 times for taking the average). After recording resting potential, 10-ms-duration current injection steps (2.1 Hz) with increasing strength from 10 pA to 500 pA (increments of 10 pA) were applied in the current clamp. The rheobase was defined as the current intensity at which the neuron reliably fired an action potential ($V_{peak} > 0$ mV), and the rheobase density was defined as rheobase divided by the membrane capacitance. The amplitude, maximal rising speed, and threshold voltage (defined as the membrane potential when the spike onset slope first reached 10 mV/ms) are all calculated from this first action potential. For measuring the relationship between spike frequency and stimulation strength, 500-ms-duration current steps (1 Hz) from 5 pA to 100 pA

(increments of 5 pA) were applied to the cells after the 10-ms-duration stimulation. The resting potential of each neuron was recorded before all current injections.

The whole-cell voltage clamp experiments were performed in an extracellular buffer consisting of 140 mM NaCl, 3 mM KCl, 1 mM $MgCl_2$, 1 mM $CaCl_2$, 10 mM glucose, and 10 mM HEPES. The pH was adjusted to 7.3 with 5 M NaOH, and osmotic pressure was adjusted to 305–315 mOsm/kg with 1 M glucose, respectively. The internal solution consisting of 140 mM CsCl (Sigma-Aldrich), 10 mM NaCl, 2 mM $MgCl_2$, 0.1 mM $CaCl_2$, 1.1 mM EGTA, and 10 mM HEPES, and its pH and osmotic pressure were adjusted to 7.3 with 50 wt. % CsOH (Sigma-Aldrich) and 290–300 mOsm/kg with 1 M sucrose. Before the test, 20 mM TEA-Cl (voltage-gated K^+ channels inhibitor, Sigma-Aldrich) and 0.1 mM $CdCl_2$ (voltage-gated Ca^{2+} channels inhibitor, Aladdin) were added into the extracellular buffer for voltage-gated Na^+ channels measurement. After calculating the series resistance, the neurons' membrane resistance, and membrane capacitance, as mentioned in the last paragraph, neurons were held at – 80 mV and 500-ms-duration voltage change pulse steps (1 Hz) from -100 mV to 60 mV (increments of 5 mV) were applied to clamped cells to record the I_{max} at each membrane potential for plotting the I-V curve. The voltage threshold was defined as the membrane potential at the first current (Iden >10 pA/pF) observed in the voltage change pulse steps.

QUANTIFICATION AND STATISTICAL ANALYSIS

Analysis of proximity labeling specificity and efficiency in the AIS

Cortical neurons of DIV10-14 were processed for optimizing AIS proximity labeling parameters. AIS was defined by endogenous NF186. Biotinylated proteins signal in the AIS and soma was quantified. Correct mean intensity (CMF) was obtained after extracting mean background. Labeling efficiency was evaluated by the AIS CMF. Labeling specificity was evaluated by the ratio of AIS CMF/ Soma CMF. At least two times independent experiments were performed.

Analysis of polarity index of novel AIS proteins

Developmental neurons fixed at DIV6, 15 or 21 were used for PHGDH and SCRIB polarity distribution study. AIS was defined by AnkG or TRIM46. A 10-pixel line was drawn along the AIS, the axon (40 μm away from the distal end of the AIS), or the proximal dendrites (similar width) and the intensity was measured. Background was extracted and the correct mean intensity (CMF) of targets was used for polarity index evaluation: AIS/Axon ratio= AIS CMF/ Axon CMF; AIS/Dendrite ratio= AIS CMF/ Dendrite CMF. Two times independent experiments were performed.

Quantitative analysis of AIS components and AIS length changes

Cortical neurons at DIV11-19 were used for pharmacology experiments. After treatment with PHGDH inhibitors or non-active analogue/ solvent, samples in treated condition or control condition were experienced the same workflow for manipulations including imaging. Images were acquired in focal position of target channels for quantification. A 10-pixel line was drawn along the AIS using Fiji-ImageJ software (NIH). AIS start and end position were distinguished by eyes as images were adjusted with the same displayed value in ImageJ. Integrated intensity of AIS components (e.g. AnkG, NF186 and TRIM46) and AIS length were measured. Correct total fluorescence (CTF) of AIS components was calculated based on the formula of 'CTF= Integrated intensity - (Mean background x Area)'. To better compare the changes of AIS structure, normalized AIS length and compositions against that in control were pooled together from independent experiments. At least two times independent experiments were performed.

Statistical analysis

All statistical analyses were performed in GraphPad Prism 8. Data were collected and analyzed from at least two independent experiments. The statistical details including the

number of experiments, number of cells and statistical tests can be found in figure legends. Normal distribution test was first applied to statistical data using the D'Agostino and Pearson omnibus test or Shapiro-Wilk test. Statistical analysis was performed by two tailed t-test for two group comparisons: Unpaired t-test for parametric data and Mann-Whitney test for non-parametric data. For multiple group comparisons, One-way analysis of variance with Tukey test or Kruskal-Wallis with Dunn's correction test was performed for parametric and non-parametric data, respectively. Graphs are presented as the mean ± SEM. Differences were considered significant when p-value less than 0.05, and represented as: *$p<0.05$, **$p<0.01$, ***$p<0.001$ and ****$p< 0.0001$.

METHOD REFERENCES

1. Kaech, S., and Banker, G. (2006). Culturing hippocampal neurons. Nature protocols *1*, 2406-2415. 10.1038/nprot.2006.356.
2. Zhang, W., Bonadiman, A., Ciorraga, M., Benitez, M.J., and Garrido, J.J. (2019). P2Y1 Purinergic Receptor Modulate Axon Initial Segment Initial Development. Frontiers in cellular neuroscience *13*, 152. 10.3389/fncel.2019.00152.
3. Frankenfield, A.M., Fernandopulle, M.S., Hasan, S., Ward, M.E., and Hao, L. (2020). Development and Comparative Evaluation of Endolysosomal Proximity Labeling-Based Proteomic Methods in Human iPSC-Derived Neurons. Analytical chemistry *92*, 15437-15444.
4. Aguilan, J.T., Kulej, K., and Sidoli, S. (2020). Guide for protein fold change and p-value calculation for non-experts in proteomics. Molecular Omics *16*, 573-582.
5. Garrido, J.J., Giraud, P., Carlier, E., Fernandes, F., Moussif, A., Fache, M.-P., Debanne, D., and Dargent, B. (2003). A targeting motif involved in sodium channel clustering at the axonal initial segment. Science *300*, 2091-2094.
6. Gao, Y., Hisey, E., Bradshaw, T.W., Erata, E., Brown, W.E., Courtland, J.L., Uezu, A., Xiang, Y., Diao, Y., and Soderling, S.H. (2019). Plug-and-play protein modification using homology-independent universal genome engineering. Neuron *103*, 583-597. e588.
7. Ogawa, Y., and Rasband, M.N. (2021). Endogenously expressed Ranbp2 is not at the axon initial segment. Journal of cell science *134*, jcs256180.